AFRL-SR-BL-TR-98-

0507

REPORT DOCUMENTATION F

1. AGENCY USE ONLY (Leave blank)	2. REPORT DATE	3. REPORT TYPE AND DATES COVERED
		01 Jun 95 to 31 May 98 Final

4. TITLE AND SUBTITLE
(AASERT-95) Noise Characterization of Devices [redacted]s for Optical Computing

5. FUNDING NUMBERS
61103D
3484/TS

6. AUTHOR(S)
Professor Walkup

7. PERFORMING ORGANIZATION NAME(S) AND ADDRESS(ES)
Texas Tech University
P O Box 4439
Lubbock TX 79409-4439

8. PERFORMING ORGANIZATION REPORT NUMBER

9. SPONSORING/MONITORING AGENCY NAME(S) AND ADDRESS(ES)
AFOSR/NE
110 Duncan Ave RMB115
Bolling AFB DC 20332-8050

10. SPONSORING/MONITORING AGENCY REPORT NUMBER
F49620-95-1-0402

11. SUPPLEMENTARY NOTES

12a. DISTRIBUTION/AVAILABILITY STATEMENT
APPROVAL FOR PUBLIC RELEASED: DISTRIBUTION UNLIMITED

12b. DISTRIBUTION CODE

13. ABSTRACT *(Maximum 200 words)*

The major objective of the research effort is to investigate the noise characteristics of advanced optical sources, spatial light modulators, and other devices which are candidates for applications in optical computers. In the past three years we have made progress in two main areas: developed and refined a Volterra Series-based nonlinear model for optical devices, and additional measurements on real optical spatial light modulators.

19980630 043

14. SUBJE

15. NUMBER OF PAGES

16. PRICE CODE

17. SECURITY CLASSIFICATION OF REPORT	18. SECURITY CLASSIFICATION OF THIS PAGE	19. SECURITY CLASSIFICATION OF ABSTRACT	20. LIMITATION OF ABSTRACT
UNCLASSIFIED	UNCLASSIFIED	UNCLASSIFIED	UL

NSN 7540-01-280-5500

Standard Form 298 (Rev. 2-89)
Prescribed by ANSI Std. 239-18

Noise Characterization of Devices for Optical Computing

Final Technical Report

on

AFOSR Grant F49620-95-1-0402

Co-Principal Investigators: John F. Walkup, Thomas F. Krile and David J. Mehrl

Submitted to

AFOSR/NE
110 Duncan Ave., Suite B115
Bolling AFB, DC 20332-0001
Attn: Dr. Alan E. Craig

by the

Optical Systems Laboratory
Department of Electrical Engineering
Texas Tech University
Lubbock, TX 79409-3102

Period Covered: June 1, 1995 through May 31, 1998

Date Submitted: June, 1998

Introduction:

This is the final technical report on AFOSR AASERT Grant F49620-95-1-0402 (June 1, 1995 through May 31, 1998, $116,936) entitled "Noise Characterization of Devices for Optical Computing". There is also a core Grant F49620-95-1-0140 (January 15, 1995 through May 31, 1998, $418,671) under the direction of Drs. Walkup and Krile. The final report on the core grant is being submitted as a separate report.

Objectives:

The major objective of the research effort is to investigate the noise characteristics of advanced optical sources, spatial light modulators, and other devices which are candidates for applications in optical computers. Obtaining good noise models will enable investigators to predict system performance, including mean square errors, bit error rates, and other performance measures.

Overview of the Effort:

In the past three years we have made progress in two main areas: developed and refined a Volterra Series-based nonlinear model for optical devices, and additional measurements on real optical spatial light modulators. Measurements of the noise characteristics of a Hughes Liquid Crystal Light Valve were reported at the SPIE 1996 Annual Meeting in Denver in August, 1996. Our modeling strategy will enable us to determine linear and nonlinear operating characteristics, as well as models for noise and crosstalk, of devices useful for applications in optical computing and communication systems. A number of pieces of measurement equipment were acquired and have been used in the experiments on various spatial light modulators and optical sources.

Summary of Accomplishments:

See the section "Noise Characterization of Devices for Optical Computing" which follows. This summarizes the accomplishments during the three year grant period. Also see the paper preprints in the Appendix.

Noise Characterization of Devices for Optical Computing

Abstract

Our approach to the noise characterization of optical devices is to first model the device as a nonlinear, multiple-input, single-output system. This system model serves as a basis for characterizing the signal and noise performance of the optical device. Here we review our accomplishments in this study. We report discoveries made since prior progress reports and outline future publication and research plans.

Accomplishments

We view the optical devices as "black box" systems where the inputs and outputs are related to each other by an explicit mathematical operation. The first model we investigated for optical devices was a multiple-input Taylor Series expansion about an operating point. This model is described in previous reports and in a paper presented to the SPIE 1996 Conference on Materials, Devices, and Systems for Optoelectronic Processing entitled "Multiport Model of a Liquid Crystal Light Valve." That paper was included as an appendix to a previous report. In addition we describe in that paper a noise immune measurement technique using sinusoidal stimulation and synchronous detection with a lock-in amplifier. We performed several preliminary experiments using a Hughes 4050 liquid crystal light valve to confirm the

feasibility of this approach to characterizing optical devices. The results of these experiments are shown in the SPIE Conference paper mentioned above. From these experiments we have drawn several conclusions. The first conclusion is that the nonlinear multiport network approach to optical devices is reasonable. We observed the multiple port effects and nonlinear effects we anticipated by applying the Taylor Series expansion model. In addition, for the Hughes liquid crystal light valve, we observed that a second order nonlinear approximation accounts for the majority of the nonlinear effects.

The Taylor Series is limited in that it only describes the steady state sinusoidal response of a system at a single frequency. To model the complete response of a nonlinear system it is necessary to use a Volterra Series, which has been described as a "Taylor Series with memory" and has the same convergence properties as a Taylor Series. The Volterra Series is a generalization of the approach used in linear system analysis that uses a summation of nonlinear impulse responses to approximate the response of a nonlinear system to an arbitrary input. The mathematical expression of the Volterra Series is detailed in our paper accepted for publication in a special issue of Applied Optics on spatial light modulators entitled "Volterra Series Modeling of Spatial Light Modulators." This paper is scheduled for publication in November. A pre-print of this paper is included as an appendix to this report.

Since the Volterra series is a generalization and extension of conventional linear systems analysis, it takes a form analogous to linear systems analysis. The nonlinear system is described by a sum of the outputs of N nonlinear elements, also known as Volterra kernels. Each of the nonlinear elements is defined by a nonlinear impulse response. The output of each

nonlinear element is determined by a multi-dimensional convolution integral. The first-order Volterra kernel is simply the response of a linear time invariant system defined by the conventional convolution integral. The second-order term is defined by a two-dimensional convolution integral, and the nth term is defined by an n-dimensional convolution integral. Weakly nonlinear devices may be adequately represented by Volterra series of low order. Based on our observations in preliminary experiments we have limited ourselves to a second order Volterra Series.

Just as in linear time invariant systems, these nonlinear impulse response functions may be transformed into multidimensional nonlinear transfer functions. A nonlinear system may be approximated by a set of nonlinear transfer functions that corresponds to the set of Volterra kernels. Measurement of the set of transfer functions describes the nonlinear system and provides a tool to analyze the signal and noise performance of the optical device and examine nonlinear effects. In addition, after an accurate estimation of the transfer function has been measured, the transfer function may be transformed to find the nonlinear impulse responses.

We investigated different experimental methods of measuring the transfer functions of optical devices using a second order Volterra Series model. A method using sinusoidal inputs and synchronous detection is detailed in the Applied Optics paper mentioned above. We show there that the nonlinear transfer functions may be directly measured using this technique. A second method we investigated involves using random broad-band signals as inputs to a discrete time Volterra series model.

We outlined a discrete-time Volterra series model in a previous report. The discrete-time model is an extension of discrete-time linear system models. The system may also be described by formulating the current output as a function of past outputs as well as current and past inputs. This is the approach commonly used in discrete linear systems. This method when applied to nonlinear systems has been called the NARMAX model (for Nonlinear AutoRegressive Moving Average with eXogenous inputs). This formulation is also detailed in a previous report. The advantage of the NARMAX model is a reduction in the number of parameters required to describe the system. The system parameters may be estimated through a method involving a Gram-Schmidt orthogonalization of the actual input and output data. This method is outlined in a previous report and was shown as a poster presentation at the 1997 OSA Annual Meeting in Long Beach CA. Once the discrete-time model has been estimated, the continuous-time nonlinear transfer functions may be calculated.

Discoveries

There is no universally applicable method to modeling nonlinear systems. Each model is typically system specific, and must be tailored to the characteristics of each system. Consequently an a priori knowledge of a specific nonlinear system is very useful in determining the appropriate mathematical model for that system and the measurement technique that may better measure the system parameters. We have investigated the type of model we would expect to find for a liquid crystal light valve. We have found this device to be essentially a mixer. In like manner an a priori knowledge of the characteristics of nonlinear systems is useful in matching the models to

measured nonlinear system characteristics. We investigated the form of a general nonlinear system using a linear-nonlinear-linear block approach. By comparing anticipated nonlinear transfer functions with actual measurements, the form of the nonlinear transfer function may be deduced.

We have applied these findings to the measurement of the nonlinear transfer functions of a liquid crystal light valve. The results of these measurements are shown in the Applied Optics paper mentioned above and appended to this report. This paper includes measured nonlinear transfer functions where they are easily made. The measurements are used to determined the form of the two-dimensional nonlinear transfer functions, and an estimated function is calculated based on measured data. We show in this paper how the Volterra series approach may be applied to a typical optical device, and the results that may be obtained.

We have investigated the noise transformation properties of nonlinear systems. The results are outlined in a paper presented to the 1998 SPIE Annual International Symposium on Aerospace/Defense Sensing, Simulation and Controls entitled "Noise characterization of a liquid crystal light valve using a multiple-port Volterra series model." This study shows how the power spectral density of the output of a nonlinear system is related to the power spectral density of the inputs to the nonlinear system. We find that the nonlinear transfer functions are used in calculating the spectral power density of the system output. This connects our modeling and parameter measurement techniques directly to the analysis of the noise characteristics of the device under study. If the inputs to a nonlinear system are independent, we have calculated the

power spectral density of the total system to be the sum of the power spectral densities of each of the nonlinear transfer functions used in the system model.

We have made preliminary noise measurements of a liquid crystal light valve using random signal inputs. We have noted how the noise propagates from each of the inputs to the output. These measurements are outlined in the SPIE paper mentioned above. These measurements show the susceptibility of noise in the output signal to noise in each of the input signals.

Our research will make the connection between the modeling and parameter measurement techniques and the noise characterization of the optical devices. We plan to use the measured nonlinear transfer functions to calculated the anticipated noise characteristics of optical devices and compare the theoretical predictions with measured results. These experiments and calculations will be presented in a paper in preparation for publication in Applied Optics or Optical Engineering and in a doctoral dissertation.

Bibliography

1. E. Bedrosian and S. O. Rice, "The Output Properties of Volterra Systems (Nonlinear Systems with Memory) Driven by Harmonic and Gaussian Inputs," Proceedings of the IEEE, 59, 1688-1707 (1971).

2. J. S. Bendat, Nonlinear System Analysis and Identification from Random Data, John Wiley and Sons, Inc., New York (1990).

3. S. A. Billings and K. M. Tsang, "Spectral analysis for non-linear systems, Part I: Parametric non-linear spectral analysis," Mechanical Systems and Signal Processing, 3, 319-339 (1989).

4. S. A. Billings and K. M. Tsang, "Spectral analysis for non-linear systems, Part II: Interpretation of non-linear frequency response functions," Mechanical Systems and Signal Processing, 3, 341-359 (1989).

5. S. A. Billings and W. S. F. Voon, "Correlation based model validity tests for non-linear models," International Journal of Control, 44, 235-244 (1985).

6. S. A. Billings and M. I. Yusof, "Decomposition of generalized frequency response functions for nonlinear systems using symbolic computation," International Journal of Control, 65, 589-618 (1996).

7. S. A. Billings and Q. M. Zhu, "Nonlinear model validation using correlation tests," International Journal of Control, 60, 1107-1120 (1994).

8. S. Boyd, Y. S. Tang and L. O. Chua, "Measuring Volterra Kernels," IEEE Transactions on Circuits and Systems, 30, 571-577 (1983).

9. S. Chen and S. A. Billings, "Representations of non-linear systems: the NARMAX model," International Journal of Control, 49, 1013-1032 (1989).

10. C. Evans, D. Rees, L. Jones and M. Weiss, "Periodic signals for measuring nonlinear Volterra kernels," IEEE Transactions on Instrumentation and Measurement, 45, 362-371 (1996).

11. A. S. French and E. G. Butz, "Measuring the Wiener kernels of a non-linear system using the fast Fourier transform algorithm," International Journal of Control, 17, 529-539 (1973).

12. R. Haber, "Structural identification of quadratic block-oriented models based on estimated Volterra kernels," International Journal of System Science, 20, 1355-1380 (1989).

13. M. J. Korenberg, "Identifying nonlinear difference equation and functional expansion representations: The fast orthogonal algorithm", Annals of Biomedical Engineering, 16, 123-142 (1988).

14. M. J. Korenberg, "A robust orthogonal algorithm for system identification and time-series analysis", Biological Cybernetics, 60, 267-276 (1989).

15. M. J. Korenberg, S. B. Bruder and P. J. McIlroy, "Exact orthogonal kernel estimation from finite data records: Extending Wiener's identification of nonlinear systems", Annals of Biomedical Engineering, 16, 201-214 (1988).

16. M. J. Korenberg and L. D. Paarmann, "Orthogonal approaches to times-series analysis and system identification," IEEE Signal Processing Magazine, 8, 29-43 (1991).

17. T. Larsen, "Determination of Volterra Transfer Functions of Non-linear Multiport Networks," International Journal of Circuit Theory and Applications, 21, 107-131 (1993).

18. T. Larsen, "Theory of Weakly Non-linear Noisy Systems," International Journal of Circuit Theory and Applications, 19, 431-452 (1991).

19. Y. W. Lee and M. Schetzen, "Measurement of the Wiener kernels of a non-linear system by cross-correlation," International Journal of Control, 2, 237-254 (1965).

20. G. Palm and T. Poggio, "The Volterra representation and the Wiener expansion: Validity and pitfalls", SIAM Journal of Applied Mathematics, 33, 195-216 (1977).

21. G. Palm, "On representation and approximation of nonlinear systems", Biological Cybernetics, 31, 119-124 (1978).

22. J. C. Peyton Jones and S. A. Billings, "Interpretation of non-linear frequency response functions," International Journal of Control, 52, 319-346 (1990).

23. J. C. Peyton Jones and S. A. Billings, "Recursive algorithm for computing the frequency response of a class of non-linear difference equation models," International Journal of Control, 50, 1925-1940 (1989).

24. M. Rudko and D. D. Weiner, "Volterra Systems with Random Inputs: A Formalized Approach," IEEE Transactions on Communications, COM-26, 217-227 (1978).

25. W. J. Rugh, Nonlinear System Theory: The Volterra/Wiener Approach, Johns Hopkins University Press, Baltimore, Maryland (1981).

26. M. Schetzen, The Volterra and Wiener Theories of Nonlinear Systems, John Wiley and Sons, Inc., New York (1980).

27. M. Schetzen, "A theory of non-linear system identification", International Journal of Control, 20, 577-592 (1974).

28. K. M. Tsang and S. A. Billings, "Reconstruction of linear and non-linear continuous time models from discrete time sampled-data systems," Mechanical Systems and Signal Processing, 6, 69-84 (1992).

29. K. M. Tsang and S. A. Billings, "Identification of linear and nonlinear continuous time models from sampled data sets," Journal of Systems Engineering, 5, 249-267 (1995).

30. D. D. Weiner and J. F. Spina, Sinusoidal Analysis and Modelling of Weakly Nonlinear Circuits, Van Nostrand Reinhold Co., New York (1980).

31. R. E. Wickesberg and C. D. Geisler, "Artifacts in Wiener kernels estimated using Gaussian white noise", IEEE Transactions on Biomedical Engineering, BME-31, 454-461 (1984).

32. Y. Yokota, N. Toda and S. Usui, "Precision analysis of Wiener kernels measured by cross-correlation method," Electronics and Communication in Japan, Part 3, 76, 13-22 (1993).

Personnel:

1. Faculty:

Dr. J.F. Walkup, Co-Principal Investigator, P.W. Horn Professor

Dr. T.F. Krile, Co-Principal Investigator, Professor

Dr. D. J. Mehrl, Co-Investigator, Associate Professor (Chairman of Mark Storrs' Ph.D. dissertation committee).

2. Graduate Student:

S. Mark Storrs, Ph.D. student

3. Secretary:

E. Gonzales

Publications during the grant period:

Journal Publications:

Journal papers published or accepted:

M. Storrs, D. J. Mehrl and J.F. Walkup, "Programmable Spatial Filtering with Bacteriorhodopsin", Appl.Optics,35, 4632-4636 (1996).

M. Storrs, D.J. Mehrl, J.F. Walkup and T.F. Krile, "Volterra Series Model of Spatial Light Modulators," (in press for special issue of Appl.Optics-Information Processing,1998).

Journal papers in preparation:

M.Storrs et.al., paper entitled "Noise Characteristics of a Liquid Crystal Light Valve" in preparation for publication in either Applied Optics or Optical Engineering.

Ph.D. dissertation in preparation:

S.M. Storrs , "Noise Characterization Of Devices For Optical Computing," Texas Tech University, 1998.

Interactions/Transitions:

Conferences/Seminars/Briefings

1. Presented invited colloquium entitled "Performance Enhancement in Optical Computing", Penn State University, State College, PA, September, 1995 (J.F. Walkup).

2. Participated in Phoenix, AZ Workshop(March 27-28, 1996) on Data-Encoding for Page-Oriented Optical Memories (Drs. Walkup, Krile, and graduate student Jin Choi). Dogan Timucin (NASA Ames) presented a paper based on previous Texas Tech AFOSR-funded work relating to statistical models for optical 3-plane processors.

3. Attended SPIE Aerosense '96, Orlando, FL, and presented paper entitled "Holographic data storage in bacteriorhodopsin using phase-encoded multiplexing and spectrum spreading techniques", April, 1996 (T.F. Krile and J.Y. Choi).

4. Attended SPIE Aerosense '96. Orlando, FL, and presented paper entitled "Application of Multiple Error Correcting Binary BCH Codes to Optical Matrix-Vector Multipliers" (T.F. Krile).

5. Attended SPIE Annual Meeting, Denver, CO and presented paper entitled "Multiport Model of a Liquid Crystal Light Valve", August, 1996 (J.F. Walkup and M. Storrs).

6. Participated in panel discussion on Future Directions for Optical Signal Processing and Computing, SPIE Annual Meeting, Denver, CO, August, 1996 (J.F. Walkup).

7. Attended OSA Annual Meeting, Rochester, NY, October, 1996 (J.F. Walkup and T.F. Krile).

8. Presented paper entitled "Noise Modeling of a Photon Echo Memory in the Frequency Domain" at the 1996 LEOS meeting in Boston, MA, Nov. 1996 (Jin Choi).

9. Attended Gordon Research Conference on Optical Signal Processing and Holography, June, 1997 (J.F. Walkup). Presented poster paper on "Laser Noise Analysis for a Photon Echo Memory".

10. Attended 1997 SPIE Annual Technical Symposium, San Diego, CA, July, 1997 (J.F. Walkup and T.F. Krile). Dr. Walkup received SPIE Fellow award.

11. Presentation to the Amarillo TX Section of the IEEE entitled "Mathematical Models of Optical Devices," September 18, 1997(S.M. Storrs).

12. Presented paper "Hologram Multiplexing in Bacteriorhodopsin," OSA Annual Meeting, Long Beach, CA, October 1997 (A.S. Bablumian, T.F. Krile, D.J. Mehrl, J.F. Walkup).

13. Presented paper "Noise Characteristics of a Photon Echo Memory," OSA Annual Meeting, Long Beach, CA, October 1997 (J.Y. Choi, J.F. Walkup,T.F. Krile, and D.J. Mehrl).

14. Presented paper "Applications of Bacteriorhodopsin for Optical Data Storage and Processing,"(invited), LEOS '97, San Francisco, CA, November 1997(A. S.Bablumian, D.J. Mehrl, T.F. Krile, J.F. Walkup).

15. Plan to present paper "Holographic Multiplexing in a Multilayer Recording Medium", SPIE Vol. 3468, SPIE Annual Meeting, San Diego, CA, July, 1998 (A.S. Bablumian, T.F. Krile, D.J. Mehrl and J.F. Walkup).

16. Plan to present paper "Bit Error Rates for a Photon-echo Memory," SPIE Vol. 3468, SPIE Annual Meeting, San Diego, CA, July, 1998 (J.Y. Choi, J.F. Walkup, T.F. Krile and D.J. Mehrl).

17. Plan to present paper "Volterra Series Model and Output Statistics of a Liquid Crystal Light Valve " at OSA Annual Meeting, Baltimore, MD, October, 1998 (S.M. Storrs, D. J. Mehrl, T.F. Krile and J.F. Walkup).

Lab Visits and Interaction

1. Visited SRI International for meetings with members of Dr. Ravinder Kachru's group in Molecular Physics Laboratory, February, 1997 (Drs. J.F. Walkup and D.J. Mehrl, Ph.D. student J.Y. Choi). Also visited NASA Ames for discussions related to research on holographic data storage in Bacteriorhodopsin.

2. Interacted with Dr. Henryk Temkin, Maddox Chair Professor at Texas Tech University on noise modelling for optical sources and devices (1997-98).

Transitions

Dr. Temkin, Dr. Kachru and other researchers are interested in our noise models, and actively collaborated with us. Further collaboration is anticipated in future years.

New Discoveries, Inventions or Patents: No inventions or patents during this funding period. See following writeups for details on results obtained.

Honors/Awards:

John F. Walkup: Fellow of IEEE, Optical Society of America, and SPIE. P.W. Horn Professor of Electrical Engineering at Texas Tech University.

Thomas F. Krile: Fellow of Optical Soc. of America. Various teaching and research awards from Texas Tech University.

David J. Mehrl: Various teaching and research awards from Texas Tech University.

APPENDIX

"Volterra Series Modeling of Spatial Light Modulators" (to appear in Applied Optics-Information Processing, Special issue on spatial light modulators, Novermber, 1998).

"Noise characterization of a liquid crystal light valve using a multiple-port Volterra series model" (to appear in Proceedings of SPIE Vol. 3388, 1998).

Volterra Series Modeling of Spatial Light Modulators

Mark Storrs, David J. Mehrl, John F. Walkup, and Thomas F. Krile

Optical Systems Laboratory
Department of Electrical Engineering
Texas Tech University

Telephone: (806) 742-3575
Fax: (806) 742-1245
E-mail: nmstorrs@juno.com

ABSTRACT

We present a multiple-input, single-output, weakly nonlinear model of spatial light modulators using a second-order Volterra series and describe an experimental method to measure the nonlinear transfer functions using sinusoidal perturbation and synchronous detection with a lock-in amplifier. We also present an application of this method to a liquid crystal light valve.

OCIS codes: 230.3720, 230.6120.

1. INTRODUCTION

Optical information processing and optical computing systems, while benefiting from high computational speed and a high degree of parallelism, have often suffered from a lack of accuracy. In some applications a lack of accuracy may be tolerated, however progress in optical computing requires an improvement in accuracy [1]. Accuracy may be improved by developing better models of optical devices, including spatial light modulators. These device models can then be used in the design of optical information processing and computing systems to optimize the systems for accuracy. This paper presents an explicit mathematical model of spatial light modulators and presents an experimental method to measure the model parameters. The approach we adopt views the spatial light modulator as a "black box" that may be adequately described by a mathematical transformation that relates the inputs to the outputs. This is an approach often used in communications and control applications and is well suited for systems analysis. It is common to convert implicitly described building blocks into explicitly described equivalents when forming them into systems. In applying this approach to optical systems and devices, we recognize that these devices often have multiple inputs and are in many cases nonlinear. We demonstrate this approach by applying it to a liquid crystal light valve.

2. SPATIAL LIGHT MODULATOR MODEL

Consider the general, multiple-input, multiple-output system shown in Figure 1. The N-inputs and M-outputs are denoted by the vectors $\mathbf{x}(t)$ and $\mathbf{y}(t)$. They are related by the nonlinear transformation $\mathbf{T}[\cdot]$;

$$\mathbf{x}(t)=\begin{bmatrix} x_1(t) \\ x_2(t) \\ \vdots \\ x_N(t) \end{bmatrix}, \quad \mathbf{y}(t)=\begin{bmatrix} y_1(t) \\ y_2(t) \\ \vdots \\ y_M(t) \end{bmatrix}, \quad \mathbf{y}(t)=\mathbf{T}[\mathbf{x}(t)]\,. \tag{1}$$

Since this transformation is nonlinear, it is unlikely that it may be expressed exactly in a closed form. Because of this we seek a series approximation of the nonlinear transformation. Consider the general *N*-input, single output, multiple port system shown as a block-diagram in Figure 2. The multiple inputs to the system (generally all a function of time) are $x_1, x_2, \cdots, x_N$ connected to ports $P_1, P_2, \cdots, P_N$ respectively. The single output y is measured at port P_{N+1}. We assume the relationship between the inputs and the outputs may be approximated by a power series in terms of the input variables' x_1, $x_2, \cdots, x_N$. This is expressed as a Taylor series [2] expansion about an operating point as follows:

$$y(x_1, x_2, \cdots, x_N)=\sum_{m_1=0}^{\infty}\sum_{m_2=0}^{\infty}\cdots\sum_{m_N=0}^{\infty}\frac{\partial^{m_1+m_2+\cdots+m_N} f(x_{10}, x_{20}, \cdots, x_{N0})}{\partial x_1^{\,m_1}\,\partial x_2^{\,m_2}\cdots\partial x_N^{\,m_N}} \times\frac{(x_1-x_{10})^{m_1}(x_2-x_{20})^{m_2}\cdots(x_N-x_{N0})^{m_N}}{m_1!\,m_2!\cdots m_N!}, \tag{2}$$

where $x_{10}, x_{20}, \ldots, x_{N0}$ are the operating (bias) points. For a given operating point, the partial derivatives may be evaluated to a constant for each choice of indices so that the series may be represented by

$$y(x_1, x_2, \cdots, x_N)=\sum_{m_1=0}^{\infty}\sum_{m_2=0}^{\infty}\cdots\sum_{m_N=0}^{\infty} a_{m_1, m_2, \cdots, m_N} \times(x_1-x_{10})^{m_1}(x_2-x_{20})^{m_2}\cdots(x_N-x_{N0})^{m_N}, \tag{3}$$

where the constants are expressed by

$$a_{m_1, m_2, \cdots, m_N} = \frac{\partial^{m_1+m_2+\cdots+m_N} f(x_{10}, x_{20}, \cdots, x_{N0})}{\partial x_1^{m_1} \partial x_2^{m_2} \cdots \partial x_N^{m_N} \, m_1! \, m_2! \cdots m_N!}. \tag{4}$$

These coefficients define the nonlinear transformation and are functions of the operating point (x_{10}, x_{20}, $\cdots$,x_{N0}). If we assume these coefficients are scalar, we are in effect modeling the nonlinear system as a memoryless nonlinear system where the output is dependent only on the value of the inputs at each instant. This assumption is too restrictive and certainly will not lead to an accurate model of the system. Consequently we must allow the coefficients to be complex valued. In doing this we recognize that the nonlinear transformation has memory. To incorporate memory into the model, we consider the nonlinear transfer function (Volterra Series).

3 NONLINEAR TRANSFER FUNCTION MODEL OF SPATIAL LIGHT MODULATORS

Nonlinear systems with memory may be formulated in a manner that is analogous to that of linear time invariant systems. In fact linear systems are a special case of a class of problems that may be described as "generalized Fock spaces" [3]. These are Hilbert Spaces with "problem-dependent" weighted inner products and include the Volterra series. In this framework, linear and nonlinear theory can be unified. This formulation, using the Volterra series, allows one to determine the output of a nonlinear system given arbitrary inputs using convolution techniques [4] and Laplace transform techniques [5]. The Volterra Series is a generalization of the Taylor series [6,7], and has been called a

"Taylor series with memory" [8]. A Volterra series expansion can be shown to exist for a large class of time invariant [9] nonlinear systems.

The single-input, single-output Volterra description of a time-invariant nonlinear system is depicted as a block diagram in Figure 3. This system can be extended to multiple-input multiple-output [10] as well as multiple-input single-output cases. Each of the blocks in the system is defined by the nonlinear impulse response $h_n(\tau_1, \tau_2, \cdots \tau_n)$, also known as the nth order Volterra kernel, where $1 \le n \le N$. For weakly nonlinear systems, a small value of N is sufficient to describe the system. The output of the system is the sum of the nonlinear elements [6]

$$y(t) = \sum_{n=1}^{N} y_n(t) , \tag{5}$$

where the output of the nonlinear elements is determined by the convolution integrals

$$y_1(t) = \int_{-\infty}^{\infty} h_1(\tau_1)\, x(t-\tau_1)\, d\tau_1 , \tag{6}$$

$$y_2(t) = \int_{-\infty}^{\infty}\int h_2(\tau_1, \tau_2)\, x(t-\tau_1)\, x(t-\tau_2)\, d\tau_1\, d\tau_2 , \tag{7}$$

and in general,

$$y_n(t) = \int_{-\infty}\int \cdots \int^{\infty} h_n(\tau_1, \tau_2, \cdots \tau_n) \times x(t-\tau_1)\, x(t-\tau_2)\, \cdots x(t-\tau_n)\, d\tau_1\, d\tau_2\, \cdots d\tau_n . \tag{8}$$

We recognize $y_1(t)$ as the response of a linear time invariant system defined by the conventional convolution integral. The second term of the Volterra series, $y_2(t)$, is defined by a two-dimensional convolution integral, and the nth term is defined by an n-dimensional convolution integral.

The Volterra kernels possess the properties of symmetry, causality and stability [6]. The Volterra kernels are symmetric with respect to the variables of integration τ_1, τ_2, $\cdots$, τ_n so that for the second-order kernel

$$h_2(\tau_1,\tau_2) = h_2(\tau_2,\tau_1)\,. \tag{9}$$

If an unsymmetrical kernel is derived for a system, there is a process to transform it into a unique symmetric kernel [6]. To describe a causal system each of the Volterra kernels must satisfy the condition

$$h_n(\tau_1,\tau_2,\cdots\tau_n) = 0 \qquad \text{for any } \tau_i < 0,\ i = 1,\cdots,n\,. \tag{10}$$

The bounded input stability of the nonlinear operator is guaranteed if

$$\int_{-\infty}\!\!\int \cdots \int^{\infty} \left| h_n(\tau_1,\tau_2,\cdots\tau_n) \right| d\tau_1\, d\tau_2 \cdots d\tau_n < \infty\,. \tag{11}$$

Weakly nonlinear systems may be adequately represented by a truncated Volterra system. Figure 4 shows a second-order, three-input, single-output Volterra system. This model includes a first-order component for each input [$h_1(\tau)$, $h_2(\tau)$, $h_3(\tau)$], a second-order component of each input [$h_{11}(\tau_1,\tau_2)$, $h_{22}(\tau_1,\tau_2)$, $h_{33}(\tau_1,\tau_2)$] and a second-order cross-term for

each pair of inputs [$h_{12}(\tau_1,\tau_2)$, $h_{23}(\tau_1,\tau_2)$, $h_{31}(\tau_1,\tau_2)$]. The system output is the summation of these components. The output of the cross-term components is given by

$$y_{12}(t) = \int_{-\infty}^{\infty}\int h_{12}(\tau_1,\tau_2)\, x_1(t-\tau_1)\, x_2(t-\tau_2)\, d\tau_1\, d\tau_2 \,. \tag{12}$$

The cross-term, second-order, Volterra kernels may also be made symmetric with respect to τ_1 and τ_2.

Just as in linear time invariant systems, these nonlinear impulse response functions can be Fourier transformed into multidimensional transfer functions as follows [6,11]:

$$\boldsymbol{H}_1(f_1) = \int_{-\infty}^{\infty} h_1(\tau_1)\, \exp\,[-j2\pi f_1\tau_1]\, d\tau_1 \,, \tag{13}$$

$$\boldsymbol{H}_2(f_1,f_2) = \int_{-\infty}^{\infty}\int h_2(\tau_1,\tau_2)\, \exp\,[-j2\pi\,(f_1\tau_1 + f_2\tau_2)]\, d\tau_1\, d\tau_2 \,, \tag{14}$$

and in general

$$\boldsymbol{H}_n(f_1,f_2,\cdots f_n) = \int_{-\infty}^{\infty}\int \cdots \int h_n(\tau_1,\tau_2,\cdots t_n)$$

$$\times \exp\,[-j2\pi\,(f_1\tau_1 + f_2\tau_2 + \cdots f_n\tau_n)]\; d\tau_1\, d\tau_2\, \cdots d\tau_n \,. \tag{15}$$

The existence of these transforms is guaranteed for stable Volterra kernels. Because the Volterra kernel is symmetric with respect to τ_1, τ_2, $\cdots$, τ_n, the kernel transform is also symmetric with respect to $f_1, f_2, \cdots f_n$ [6] so that in the second-order case

$$\boldsymbol{H}_2(f_1,f_2) = \boldsymbol{H}_2(f_2,f_1)\,. \tag{16}$$

Since the Volterra kernel $h_n(\tau_1,\tau_2,\cdots\ \tau_n)$ is real, the complex conjugate of the second-order transfer function is

$$\boldsymbol{H}_2{}^*(f_1,f_2) = \boldsymbol{H}_2(-f_1,-f_2)\,. \tag{17}$$

Combining the symmetry and complex conjugate properties of the second-order transfer function reveals [12]

$$\boldsymbol{H}_2{}^*(f,-f) = \boldsymbol{H}_2(-f,f) = \boldsymbol{H}_2(f,-f)\,. \tag{18}$$

This demonstrates that $\boldsymbol{H}_2(-f,f)$ is a real valued even function with a phase of zero for all f. We also observe that the time domain Volterra impulse response may be found with the inverse transform

$$h_n(\tau_1,\tau_2,\cdots t_n) = \int_{-\infty}\int \cdots \int^{\infty} \boldsymbol{H}_n(f_1,f_2,\cdots f_n) \times \exp\left[j2\pi\,(f_1\tau_1 + f_2\tau_2 + \cdots f_n\tau_n)\right]\, d\tau_1\, d\tau_2\, \cdots d\tau_n\,. \tag{19}$$

For multiple input systems, such as shown in Figure 4, the cross-term transfer function is given by

$$\boldsymbol{H}_{12}(f_1,f_2) = \int_{-\infty}\int^{\infty} h_{12}(\tau_1,\tau_2)\exp\left[-j2\pi\,(f_1\tau_1 + f_2\tau_2)\right] d\tau_1\, d\tau_2\,, \tag{20}$$

which shares the symmetry properties of the single-term, second-order nonlinear transfer functions.

4. MEASURING MODEL PARAMETERS

Several methods of experimentally measuring Volterra kernels and nonlinear transfer functions have been suggested. These have been based on both random input signals and sinusoidal input signals. The measurements have resulted in both the time and frequency domain parameters. Lee and Schetzen [13] describe a method using Gaussian random inputs and time-domain correlation techniques. French and Butz [14] describe a method using random inputs and frequency domain FFT techniques. Others use discrete-time models of nonlinear systems [15] and use random inputs and orthogonalization techniques [16] to estimate the nonlinear system parameters. Here we describe a frequency domain measurement method using sinusoidal inputs to directly measure the nonlinear transfer functions using synchronous detection. The nonlinear transfer functions may be used in noise analysis and may be transformed to time-domain Volterra kernels to determine the system output to arbitrary inputs.

Applying Eq. 19 to Eq. 8 with a change of variables, we find

$$y_n(t) = \int_{-\infty}^{\infty}\cdots\int_{-\infty}^{\infty} \boldsymbol{H}_n(f_1, f_2, \cdots f_n)\, \boldsymbol{X}(f_1)\exp(j2\pi f_1 t)\, \boldsymbol{X}(f_2)\exp(j2\pi f_2 t) \times \cdots \boldsymbol{X}(f_n)\exp(j2\pi f_n t)\, df_1\, df_2 \cdots df_n , \tag{21}$$

where $\boldsymbol{X}(f)$ is the spectrum of the input signal. When the input signal is sinusoidal, that is when

$$x(t) = A\cos(2\pi f_0 t) , \tag{22}$$

where A is the amplitude of the sinusoid and f_0 is the frequency, the spectrum of the input signal is

$$\boldsymbol{X}(f) = \frac{A}{2}[\delta(f-f_0) + \delta(f+f_0)], \tag{23}$$

where $\delta(\cdot)$ is the Dirac delta function. Applying this input signal to the Volterra system described above, the first term in the series is

$$y_1(t) = \int_{-\infty}^{\infty} \boldsymbol{H}_1(f_1)\frac{A}{2}[\delta(f_1-f_0) + \delta(f_1+f_0)]\exp(j2\pi f_1 t)\, df_1 . \tag{24}$$

Carrying out the integration reveals

$$y_1(t) = \frac{A}{2}\boldsymbol{H}_1(f_0)\exp(j2\pi f_0 t) + \frac{A}{2}\boldsymbol{H}_1(-f_0)\exp(-j2\pi f_0 t) . \tag{25}$$

Applying the symmetry relationship from Eq. 18 we find

$$y_1(t) = \frac{A}{2}\boldsymbol{H}_1(f_0)\exp(j2\pi f_0 t) + \frac{A}{2}\boldsymbol{H}_1{}^*(f_0)\exp(-j2\pi f_0 t) . \tag{26}$$

By expressing the complex quantity $\boldsymbol{H}_1(f_0)$ in exponential form

$$\boldsymbol{H}_1(f_0) = |\boldsymbol{H}_1(f_0)|\exp(j\phi_1), \tag{27}$$

and then converting the expression to sinusoidal form we recognize the output of the first term of the Volterra series to take the familiar form of a linear system excited by a sinusoid

$$y_1(t) = A\ |\boldsymbol{H}_1(f_0)|\ \cos(2\pi f_0 t + \phi_1) . \tag{28}$$

With a single sinusoidal input, the second term of the Volterra series is

$$y_2(t) = \int_{-\infty}^{\infty}\int_{-\infty}^{\infty} \boldsymbol{H}_2(f_1,f_2)\frac{A}{2}[\delta(f_1-f_0)+\delta(f_1+f_0)]\frac{A}{2}[\delta(f_2-f_0)+\delta(f_2+f_0)]$$

$$\times \exp(j2\pi f_1 t)\exp(j2\pi f_2 t)\,df_1 df_2\,, \qquad (29)$$

Carrying out the multiplication and integration reveals

$$y_2(t) = \frac{A^2}{4}\boldsymbol{H}_2(f_0,f_0)\exp(j2\pi f_0 t)\exp(j2\pi f_0 t)$$

$$+\frac{A^2}{4}\boldsymbol{H}_2(-f_0,-f_0)\exp(-j2\pi f_0 t)\exp(-j2\pi f_0 t)$$

$$+\frac{A^2}{4}\boldsymbol{H}_2(-f_0,f_0)\exp(-j2\pi f_0 t)\exp(j2\pi f_0 t)$$

$$+\frac{A^2}{4}\boldsymbol{H}_2(f_0,-f_0)\exp(j2\pi f_0 t)\exp(-j2\pi f_0 t)\,. \qquad (30)$$

Applying the symmetry relationships and converting to sinusoidal form leads to the expression

$$y_2(t) = \frac{A^2}{4}\left|\boldsymbol{H}_2(f_0,f_0)\right|\cos(2\pi\, 2f_0 t + \phi_2) + \frac{A^2}{2}\left|\boldsymbol{H}_2(f_0,-f_0)\right|\,. \qquad (31)$$

We note that this results in a dc signal component and a component at twice the frequency of the sinusoidal stimulation. The total output of a truncated second-order Volterra system stimulated by a sinusoid is

$$y(t) = \left|\boldsymbol{H}_1(f_0)\right| A\cos(2\pi f_0 t + \phi_1)$$

$$+\frac{A^2}{2}\left|\boldsymbol{H}_2(f_0,f_0)\right|\cos(2\pi\, 2f_0 t + \phi_2) + \frac{A^2}{2}\left|\boldsymbol{H}_2(f_0,-f_0)\right|\,. \qquad (32)$$

We observe that the signal contains a sinusoidal component at the frequency of the input sinusoid and a sinusoidal component at twice the frequency of the input sinusoid. Furthermore the magnitude of the component at the frequency of the input signal is proportional to the first-order transfer function and the magnitude of the component at twice the frequency of the input signal is proportional to the second-order transfer function. This result suggests that we can experimentally measure the first and second-order characteristics of a weakly nonlinear device by stimulating the device with a sinusoid of known amplitude and frequency, then observing the output with a dual-channel lock-in amplifier. This approach can be applied to optical devices by impressing a sinusoidal perturbation upon one of the inputs. Figure 5 demonstrates a three-input, single-output system with a sinusoidal perturbation applied to one of the inputs and the output measured by a lock-in amplifier. When the lock-in amplifier is referenced to the frequency of the sinusoidal stimulation we measure a quantity proportional to the magnitude of the first-order Volterra transfer function. A dual-channel lock-in amplifier allows us to directly measure the phase of the Volterra transfer function. When the lock-in amplifier is referenced to twice the frequency of the sinusoidal stimulation (a feature commonly available with lock-in amplifiers) we measure the magnitude and phase of the second-order Volterra transfer function. With a single sinusoid we can measure the second-order Volterra transfer function only along the line $f_1 = f_2$. To measure the transfer function across the entire frequency plane we must apply a sum of two sinusoids at differing frequencies

$$x(t) = A\cos(2\pi f_{10} t) + B\cos(2\pi f_{20} t) \tag{33}$$

The spectrum of this input signal is

$$\boldsymbol{X}(f) = \frac{A}{2}[\delta(f-f_{10}) + \delta(f+f_{10})] + \frac{B}{2}[\delta(f-f_{20}) + \delta(f+f_{20})]\,. \tag{34}$$

The output of the second-order term is

$$\begin{aligned} y_{12}(t) = \int_{-\infty}^{\infty}\int \boldsymbol{H}_{11}(f_1,f_2)&\left[\frac{A}{2}[\delta(f-f_{10}) + \delta(f+f_{10})] + \frac{B}{2}[\delta(f-f_{20}) + \delta(f+f_{20})]\right] \\ &\times\left[\frac{A}{2}[\delta(f-f_{10}) + \delta(f+f_{10})] + \frac{B}{2}[\delta(f-f_{20}) + \delta(f+f_{20})]\right] \\ &\times \exp(j2\pi f_1 t)\exp(j2\pi f_2 t)\,df_1 df_2\,. \end{aligned} \tag{35}$$

Carrying out the multiplication and integration, then applying the symmetry rules and converting to sinusoidal form reveals

$$\begin{aligned} y_{11}(t) = \frac{A^2}{2}&|\boldsymbol{H}_{11}(f_{10},f_{10})|\cos(2\pi\, 2f_{10}t + \phi_{10}) + \frac{A^2}{4}|\boldsymbol{H}_{11}(f_{10},f_{10})| \\ &+ AB|\boldsymbol{H}_{11}(f_{10},f_{20})|\cos[2\pi\,(f_{10}+f_{20})t + \phi_{12}] \\ &+ AB|\boldsymbol{H}_{2}(f_{10},-f_{20})|\cos[2\pi\,(f_{10}-f_{20})t + \phi_{12}] \\ &+ \frac{B^2}{2}|\boldsymbol{H}_{11}(f_{20},f_{20})|\cos(2\pi\, 2f_{20}t + \phi_{20}) + \frac{B^2}{4}|\boldsymbol{H}_{11}(f_{20},f_{20})|. \end{aligned} \tag{36}$$

We observe that the complete second-order Volterra transfer function may be measured by perturbing an input with a sum of two sinusoids and referencing the lock-in amplifier to the sum (or difference) of those frequencies. This measurement is demonstrated in Figure 6. The total output of a second-order system with an input of the sum of two sinusoids as described is

$$y(t) = A\,|H_1(f_{10})|\cos(2\pi f_{10}t + \phi_1) + B\,|H_1(f_{20})|\cos(2\pi f_{20}t + \phi_2)$$

$$+\frac{A^2}{2}|H_{11}(f_{10},f_{10})|\cos(2\pi\, 2f_{10}t + \phi_{10}) + \frac{A^2}{4}|H_{11}(f_{10},f_{10})|$$

$$+AB|H_{11}(f_{10},f_{20})|\cos[2\pi\,(f_{10}+f_{20})t + \phi_{12}]$$

$$+AB|H_2(f_{10},-f_{20})|\cos[2\pi\,(f_{10}-f_{20})t + \phi_{12}]$$

$$+\frac{B^2}{2}|H_{11}(f_{20},f_{20})|\cos(2\pi\, 2f_{20}t + \phi_{20}) + \frac{B^2}{4}|H_{11}(f_{20},f_{20})|. \qquad (37)$$

By judicious selection of the two frequencies f_{10} and f_{20}, each of the signal components will exist at distinct frequencies and the first and second-order Volterra transfer functions may be measured by a lock-in amplifier. Ideally, the two frequencies should be incomensurate, however in practice it is sufficient that they be judiciously chosen so as to assure reasonable mutual separation of all frequency terms [17, 18]. In addition, because of the symmetry relationships, it is only necessary to measure data points in only one-fourth of the frequency plane. To measure the cross-term transfer functions we apply a stimulation of two sinusoids

$$x_1(t) = A\cos(2\pi f_{10}t) \text{ and } x_2(t) = B\cos(2\pi f_{20}t)\,. \qquad (38)$$

The output of the cross-term is

$$y_{12}(t) = \int_{-\infty}^{\infty}\int H_{12}(f_1,f_2)\frac{A}{2}[\delta(f_1-f_{10}) + \delta(f_1+f_{10})]\frac{B}{2}[\delta(f_2-f_{20}) + \delta(f_2+f_{20})]$$

$$\times \exp(j2\pi f_1 t)\exp(j2\pi f_2 t)\,df_1 df_2\,. \qquad (39)$$

Carrying out the multiplication and integration reveals

$$y_{12}(t) = \frac{AB}{4} \boldsymbol{H}_{12}(f_{10}, f_{20}) \exp(j2\pi f_{10}t) \exp(j2\pi f_{20}t)$$

$$+ \frac{AB}{4} \boldsymbol{H}_{12}(-f_{10}, -f_{10}) \exp(-j2\pi f_{10}t) \exp(-j2\pi f_{20}t)$$

$$+ \frac{AB}{4} \boldsymbol{H}_{12}(-f_{10}, f_{20}) \exp(-j2\pi f_{10}t) \exp(j2\pi f_{20}t)$$

$$+ \frac{AB}{4} \boldsymbol{H}_{12}(f_{10}, -f_{10}) \exp(j2\pi f_{10}t) \exp(-j2\pi f_{20}t) . \quad (40)$$

Applying the symmetry relationships and using exponential forms leads to

$$y_{12}(t) = \frac{AB}{2} |\boldsymbol{H}_{12}(f_{10}, f_{20})| \cos[2\pi(f_{10} + f_{20})t + \phi_{12}]$$

$$+ \frac{AB}{2} |\boldsymbol{H}_{12}(f_{10}, f_{20})| \cos[2\pi(f_{10} - f_{20})t + \phi_{12}] . \quad (41)$$

We note that the signal contains a component at the sum of the input sinusoid frequencies and at the difference of the input sinusoid frequencies. The magnitude and phase of the cross-term Volterra transfer function can be measured by referencing the lock-in amplifier to either the sum of the frequencies or the difference of the frequencies. This is demonstrated in Figure 7. We note that in all of these measurements we may determine the magnitude and phase of the transfer function.

5. LIQUID CRYSTAL LIGHT VALVE MODEL

The multiple port approach is well suited to describe a liquid crystal light valve (LCLV) spatial light modulator, which is by nature a nonlinear multiple port device. A functional diagram of a Hughes 4050 LCLV is shown in Figure 8 [19]. The device has three inputs; the write light, the read light and a 5 kHz AC drive signal. The liquid

crystal light valve is an optically addressed spatial light modulator that operates by spatially modulating the polarization state of the read light. Amplitude modulation is achieved by using a polarization analyzer [20].

With no write light present, the majority of the voltage from the AC drive signal drops across the photosensor and there is virtually no voltage impressed across the liquid crystal layer. The liquid crystals are aligned to undergo a 45 degree twist between the alignment layers. Linearly polarized incident light on the read side of the device will experience a 45 degree polarization rotation between the front alignment layer and the dielectric mirror. Upon reflection the light experiences a reverse 45 degree polarization rotation and exits the device in the same polarization state as the incident light. A polarization analyzer oriented at 90 degrees to the incident light will block the reflected light.

If the write side of the device is illuminated (with coherent or incoherent light) the photosensor becomes conductive with a spatial pattern dependent upon the spatial intensity distribution of the write light. Where the photosensor is conductive, a voltage is impressed across the liquid crystal layer. This voltage causes the liquid crystal molecules to tilt in the direction of the electrodes. The degree of tilt is dependent on the voltage across the liquid crystal, which in turn is dependent upon the intensity of the write light. The linearly polarized incident light is now transformed into elliptically polarized light with the degree of ellipticity dependent upon the tilt of the liquid crystal molecule. The reflected light now has a polarization component parallel to the orientation of the polarization analyzer that will be passed. The intensity of the light passed by the polarization analyzer is thus dependent on the intensity of the write light.

This spatial light modulator may be viewed as a multiple port network as illustrated in Figure 9. The input ports of the system are identified as follows:

Port 1: Write beam intensity (mW/cm^2),

Port 2: Read beam intensity (mW/cm^2),

Port 3: AC Drive (volts),

and the output port is identified:

Port 4: Photodetector current (mA).

A model of the LCLV spatial light modulator is presented in the truncated Volterra model shown in Figure 4. This model is truncated to the second-order and is posited to approximate the operation of this spatial light modulator. The output is the sum of all of these contributions.

A preliminary experimental setup to perform the lock-in amplifier measurement is shown in Figure 10. An argon ion laser beam is first conditioned by a laser intensity stabilizer then enters the experimental setup at the upper left corner. A beam splitter is positioned to divide the beam into a write beam and a read beam. An acousto-optic (AO) cell is positioned in each of the beams to provide intensity modulation of the beams. The write and read beams are expanded and passed through a 3mm iris to achieve a beam cross section of relatively constant intensity. A pair of polarizers is positioned in both the write and read beams to provide control over the intensity of the beams and to ensure linear polarization of the read beam. A beamspliter is positioned in both the write and read beams to allow measurement of the inputs to the LCLV with photodiodes. Lenses are positioned to image the iris aperture onto the LCLV write and read surfaces. A

crossed polarizer is positioned to provide intensity modulation of the read beam which is then trained onto a photodiode.

Preliminary measurements are first made with unmodulated write and read beam. The static gain of the LCLV is shown in Figure 11. The gain shown here is the ratio of the output beam intensity passed through the crossed polarizer to the intensity of the write beam. The device shows a monotonically increasing range of operation at low write beam intensity and saturation effects at higher write beam intensity. We note that near the midpoint of the monotonically increasing range it is quite reasonable to posit that the operation of the LCLV may be approximated by a second-order system. The output beam intensity is modulated by the 5 kHz AC drive signal. The first-order modulation is shown in Figure 12 and the second-order modulation is shown in Figure 13. These curves are a function of write light intensity, and represent the output power residing at the AC drive frequency (and second harmonic) as a fraction of the read beam intensity. The light modulation mechanism producing these effects is the "wobble" of the liquid crystal molecules in response to the AC drive signal. This “wobble” produces a temporal modulation of the polarization state of the reflected light, which is seen in a temporal modulation of the intensity of the light passed by the polarization analyzer. Since the liquid crystal is an induced dipole, the molecules tilt with both halves of the AC cycle, producing a modulation of the read light at twice the AC drive signal frequency. We note that at some levels of write beam intensity the second-order effects are more significant than the first-order effects. At the midpoint of the monotonically increasing range of the static operating curve (0.0005 mW/cm^2), the first-order gain is approximately 20×10^{-6}

(that is approximately -47 dB), and the second-order gain is approximately 100×10^{-6} (that is approximately -40 dB).

To measure the remaining transfer functions, we set the write beam intensity at about the midpoint of the monotonically increasing range, approximately 0.005 mW/cm^2. Modulation of the read beam showed a flat wideband first-order response shown in Figure 14. The value shown in Figure 14 is the ratio of the output beam intensity (as passed through the beam splitter and crossed polarizer) to the read beam intensity. The LCLV shows a negligible second-order response to read beam modulation. These results indicate a negligible interaction between the read beam and liquid crystal molecules.

The response to write beam modulation is very different. The first-order write beam response is shown in Figure 15 and the second-order response is shown in Figure 16. Measured data is shown in the dark line superimposed upon an estimated transfer function. The data points were measured by modulating the write beam with a sinusoid whose amplitude is approximately 10% of the dc value of the write beam, and observing the output beam intensity with a lock-in amplifier. The first-order response was measured by referencing the lock-in amplifier to the frequency of write beam modulation. The frequency of modulation was swept from 1 Hz to 1 kHz. The first-order curve is approximately that of a single pole lowpass filter with a cutoff frequency of about 6 Hz. The second-order response was measured by referencing the lock-in amplifier to twice the frequency of write beam modulation. The second-order curve is approximately that of a second-order single pole lowpass filter with a cutoff frequency of 3 Hz. We note that the second-order transfer function is two-dimensional and this measurement only detects

data points along the line $f_1 = f_2$. Since the response curve drops at 20 dB per decade (as opposed to 40 dB per decade), the second-term may be modeled as a squaring operation followed by a low-pass filter [12]. The complete second-order transfer function can be shown to take the form

$$\boldsymbol{H}_{11}(f_1, f_2) = \boldsymbol{H}(f_1+f_2)\,, \tag{42}$$

where H(f) represents the low-pass filter transfer function. Using the estimated transfer function curve shown in Figure 16. the estimated complete second-order transfer function is shown in Figure 17.

In lieu of direct measurement of the second-order cross-term transfer functions, they may be approximated from a knowledge of the LCLV operation. Since the output beam intensity is directly scaled by the read beam intensity, the modulated output beam intensity is also directly scaled by the read beam intensity. In effect this produces a multiplication operation between the write beam and the read beam. The second-order cross-term transfer function can be shown to take the form

$$\boldsymbol{H}_{12}(f_1, f_2) = \boldsymbol{H}_1(f_1)\boldsymbol{H}_2(f_2)\,. \tag{43}$$

Applying this relationship to the transfer functions shown in Figures 14 and 15, and making the function symmetrical with respect to f_1 and f_2, results in the second-order transfer function shown in Figure 18. The same relationship will hold between the AC drive and the two optical beams. The second order transfer function $\boldsymbol{H}_{23}$ will be the same form as Figure 15, scaled by $\boldsymbol{H}_3$ (-47 dB in this case) and shifted to a base frequency of 5

kHz. The second order transfer function H_{31} will be the same form as Figure 14, scaled and shifted in a similar manner.

6. CONCLUSIONS

The Volterra series appears to be a viable model for spatial light modulators that allows experimental measurement of the model parameters. The measurement method directly determines the nonlinear transfer functions. These transfer functions are applicable to noise analysis of the spatial light modulator and may be transformed to determine the response of the device to arbitrary inputs.

ACKNOWLEDGMENTS

This research was funded by the Air Force Office of Scientific Research under the Augmentation Awards for Science and Engineering Research Training (AASERT) Grant F49620-95-1-0402.

REFERENCES

1. S. G. Batsell, T. L. Jong, J. F. Walkup and T. F. Krile, "Noise limitations in optical linear algebra processors," *Applied Optics*, **29**, 2084-2090 (1990).

2. D. D. Weiner and J. F. Spina, *Sinusoidal Analysis and Modeling of Weakly Nonlinear Circuits*, Van Nostrand Reinhold Co., New York (1980).

3. R. J. P. De Figueiredo, "A Generalized Fock Space Framework for Nonlinear System and Signal Analysis," *IEEE Transactions on Circuits and Systems*, **30**, 637-647 (1983).

4. I. W. Sandburg, "A Perspective on System Theory," *IEEE Transactions on Circuits and Systems*, **31**, 88-103 (1984).

5. W. J. Rugh, *Nonlinear System Theory: The Volterra/Wiener Approach*, Johns Hopkins University Press, Baltimore, Maryland (1981).

6. M. Schetzen, *The Volterra and Wiener Theories of Nonlinear Systems*, John Wiley and Sons, Inc., New York (1980).

7. M. Schetzen, "Nonlinear System Modeling Based on the Wiener Theory," *Proceedings of the IEEE*, **69**, 1557-1573 (1981).

8. E. Bedrosian and S. O. Rice, "The Output Properties of Volterra Systems (Nonlinear Systems with Memory) Driven by Harmonic and Gaussian Inputs," *Proceedings of the IEEE*, **59**, 1688-1707 (1971).

9. I. W. Sandburg, "Expansions for Nonliner Systems," *The Bell System Technical Journal*, **61**, 159-199 (1982).

10. A. A. M. Saleh, "Matrix Analysis of Mildly Nonlinear, Multiple-Input, Multiple-Output Systems with Memory," *The Bell System Technical Journal*, **61**, 2221-2243 (1982).

11. J. C. Peyton Jones and S. A. Billings, "Interpretation of non-linear frequency response functions," *International Journal of Control*, **52**, 319-346 (1990).

12. J. S. Bendat, *Nonlinear System Analysis and Identification from Random Data*, John Wiley and Sons, Inc., New York (1990).

13. Y. W. Lee and M. Schetzen, "Measurement of the Wiener Kernels of a Non-linear System by Cross-correlation," *International Journal of Control*, **2**, 237-254 (1965).

14. A. S. French and E. G. Butz, "Measuring the Wiener kernels of a non-linear system using the fast Fourier transform algorithm," *International Journal of Control*, **3**, 529-539 (1973).

15. S. Chen and S. A. Billings, "Representations on non-linear system: the NARMAX model," *International Journal of Control*, **49**, 1013-1032 (1989).

16. M. J. Korenberg, "Identifying nonlinear difference equation and functional expansion representations: the fast orthogonal algorithm," *Annals of Biomedical Engineering*, **16**, 123-142 (1988).

17. S. Boyd, Y. S. Tang and L. O. Chua, "Measuring Volterra Kernels," *IEEE Transactions on Circuits and Systems*, **CAS-30**, 571-577 (1983).

18. C. Evans, D. Rees, L. Jones and M. Weiss, "Periodic Signals for Measuring Nonlinear Volterra Kernels," *IEEE Transactions on Instrumentation and Measurement*, **45**, 362-371.

19. J. Goodman, *Introduction to Fourier Optics*, 2nd Edition, McGraw-Hill Publishing Co., New York (1996).

20. W. P. Bleha, L. T. Lipton, E. Wiener-Avnear, J. Grinberg, P. G. Reif, D. Casasent, H. B. Brown and B.V. Markevitch, "Application of the Liquid Crystal Light Valve to Real-Time Optical Data Processing," *Optical Engineering*, **17**, 371-384 (1978).

FIGURE CAPTIONS

Figure 1: General multiple-input, multiple-output system.

Figure 2: General multiple-input, single output system.

Figure 3: Single-input, single-output Volterra system.

Figure 4: Second-order, three-input, single-output Volterra system.

Figure 5: Synchronous measurement of 1st Order Volterra transfer function.

Figure 6: Synchronous measurement of 2nd Order Volterra transfer function.

Figure 7: Synchronous measurement of 2nd Order cross-term Volterra transfer function.

Figure 8: Liquid Crystal Light Valve (LCLV).

Figure 9: LCLV Spatial Light Modulator with ports identified.

Figure 10: LCLV experimental setup.

Figure 11: LCLV Static Gain.

Figure 12: LCLV AC Drive 1st Order Transfer Function ($\boldsymbol{H}_3$).

Figure 13: LCLV AC Drive 2nd Order Transfer Function ($\boldsymbol{H}_{33}$).

Figure 14: LCLV Read Beam 1st Order Transfer Function ($\boldsymbol{H}_2$).

Figure 15: LCLV Write Beam 1st Order Transfer Function ($\boldsymbol{H}_1$).

Figure 16: LCLV Write Beam 2nd Order Transfer Function ($\boldsymbol{H}_{11}$).

Figure 17: Estimated LCLV Complete Write Beam 2nd Order Transfer Function ($\boldsymbol{H}_{11}$).

Figure 18: Estimated LCLV Write Beam-Read Beam 2nd Order Transfer Function ($\boldsymbol{H}_{12}$).

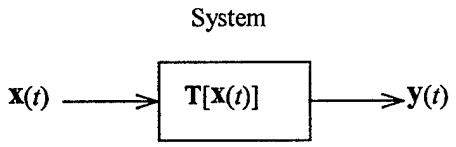

Figure 1: General multiple-input, multiple-output system.

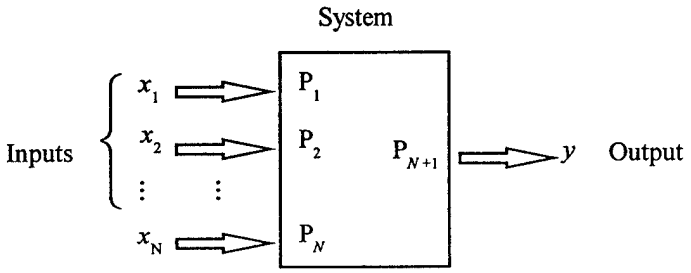

Figure 2: General multiple-input, single output system.

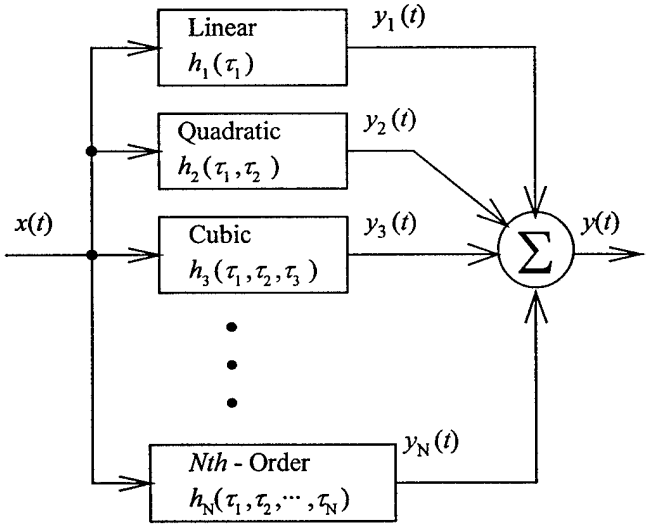

Figure 3: Single-input, Single-output Volterra system.

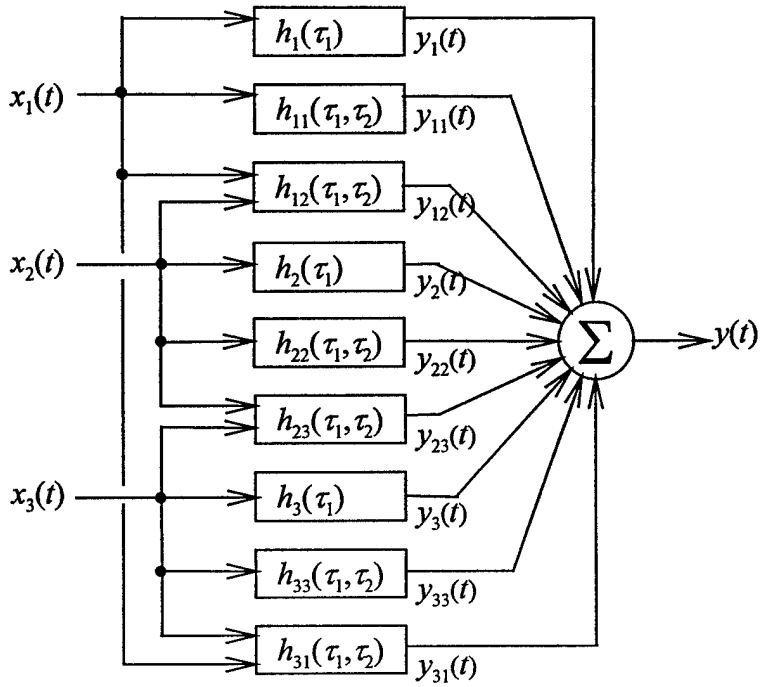

Figure 4: Second order, three-input, single-output Volterra system.

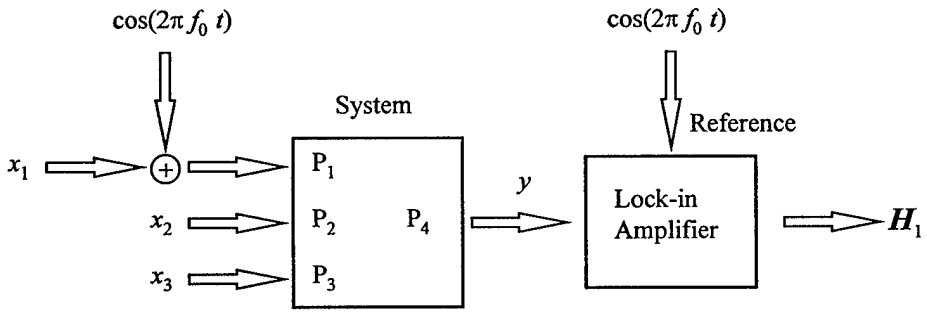

Figure 5: Synchronous measurement of 1st Order Volterra transfer function.

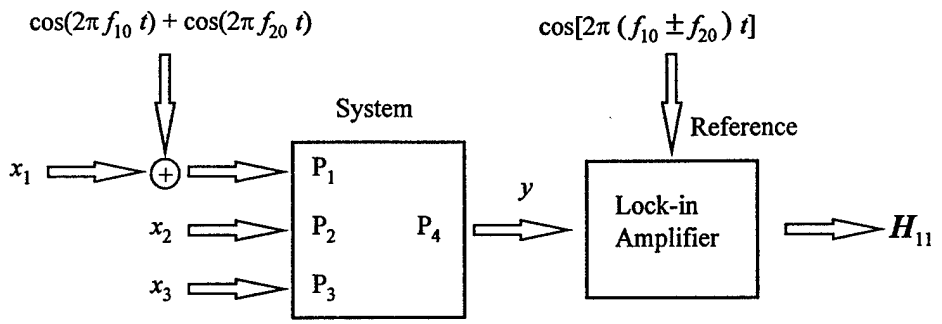

Figure 6: Synchronous measurement of 2nd Order Volterra transfer function.

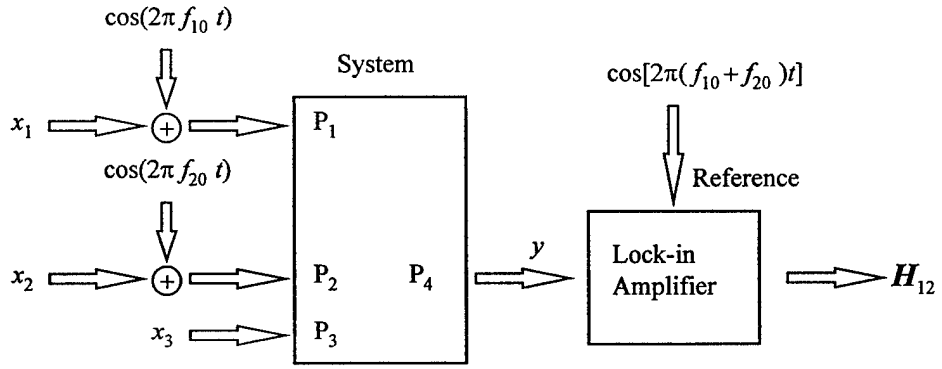

Figure 7: Synchronous measurement of 2nd Order cross-term Volterra transfer function.

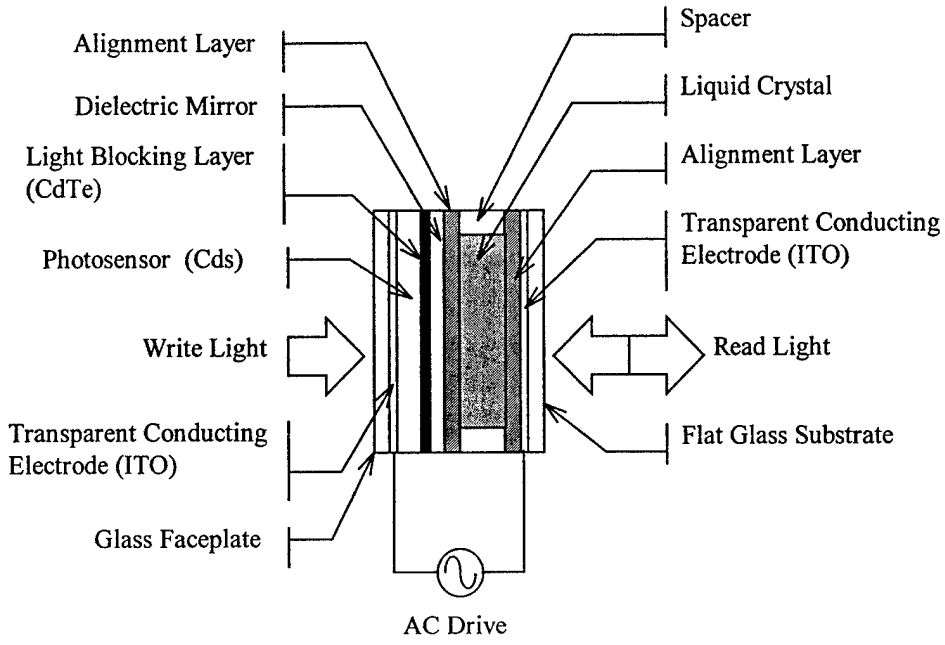

Figure 8: Liquid Crystal Light Valve (LCLV).

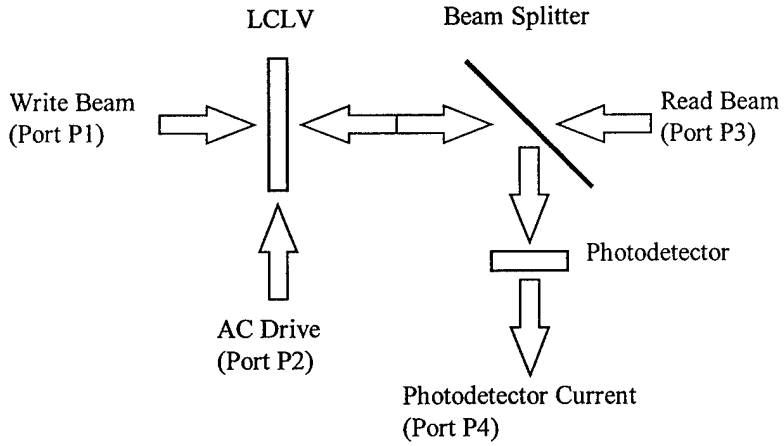

Figure 9: LCLV Spatial Light Modulator with ports identified.

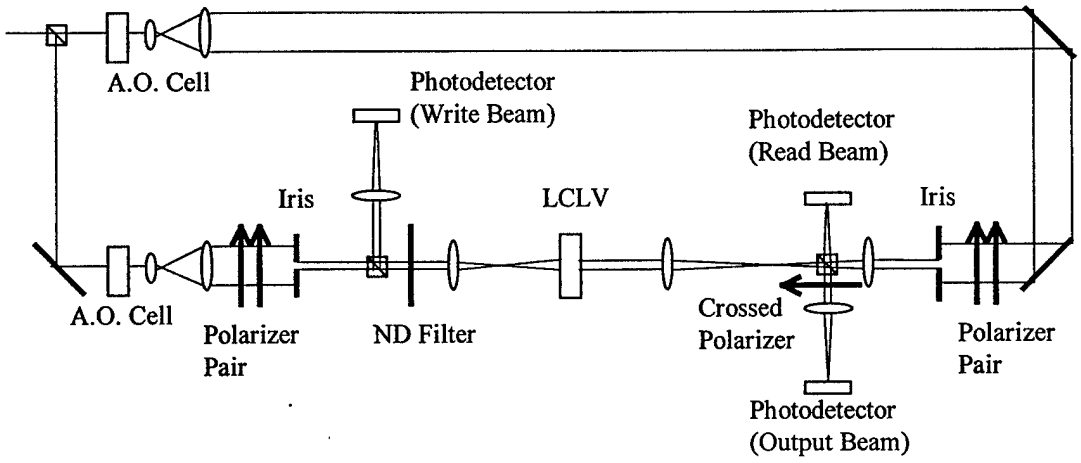

Figure 10: LCLV experimental setup.

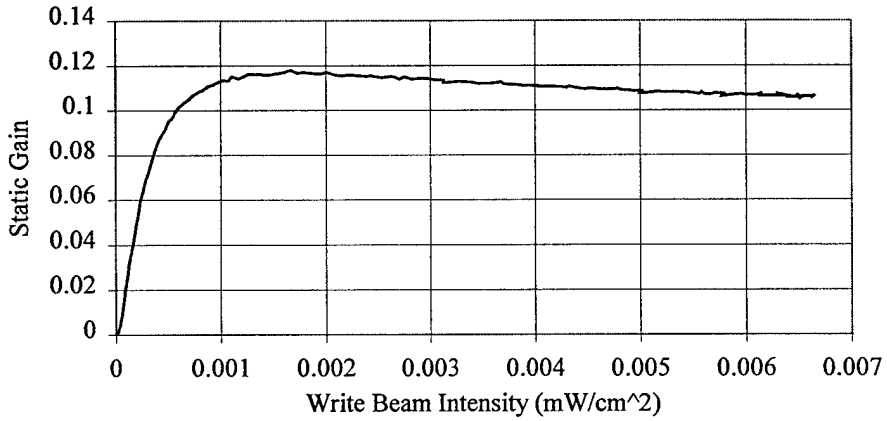

Figure 11: LCLV Static Gain.

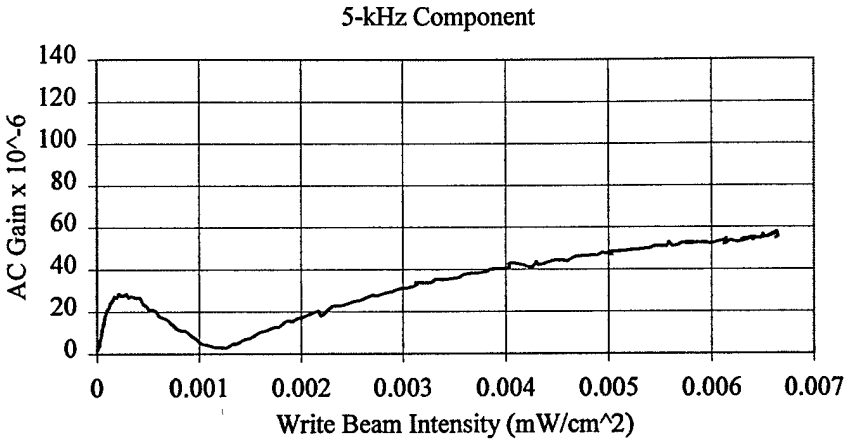

Figure 12: LCLV AC Drive 1st Order Transfer Function (H_3).

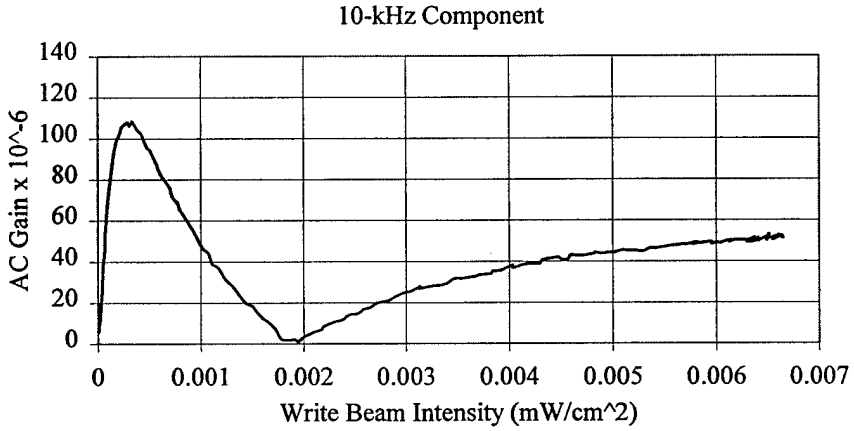

Figure 13: LCLV AC Drive 2nd Order Transfer Function (H_{33}).

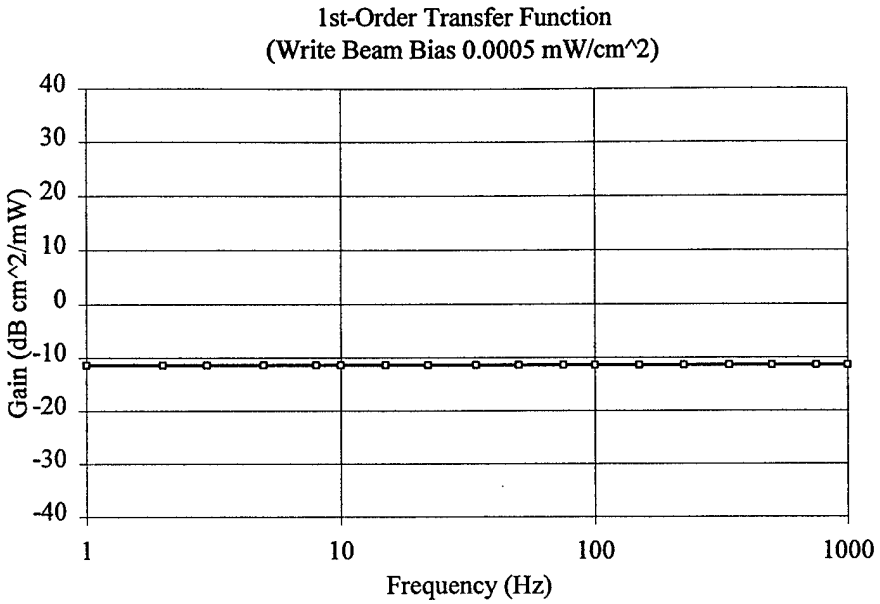

Figure 14: LCLV Read Beam 1st Order Transfer Function (H_2).

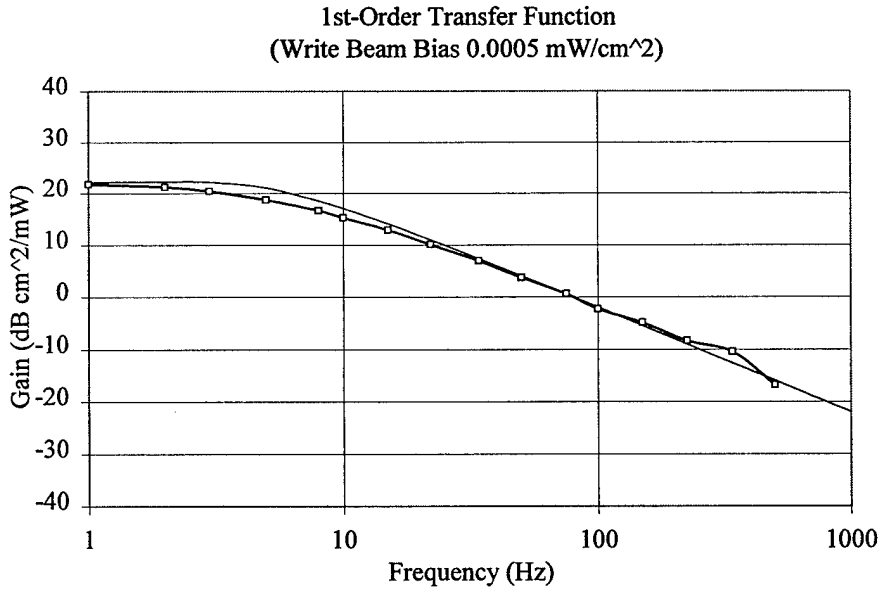

Figure 15: LCLV Write Beam 1st Order Transfer Function (H_1).

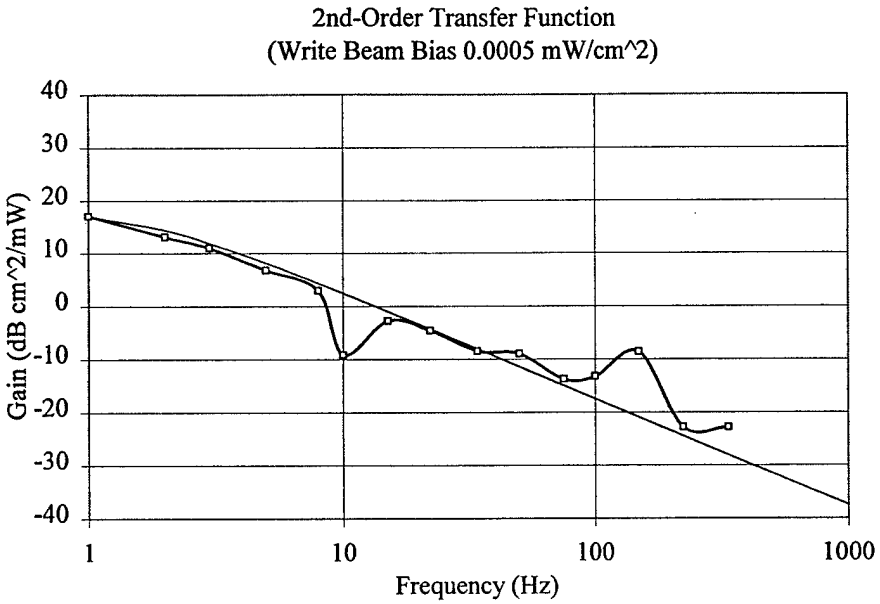

Figure 16: LCLV Write Beam 2nd Order Transfer Function (H_{11}).

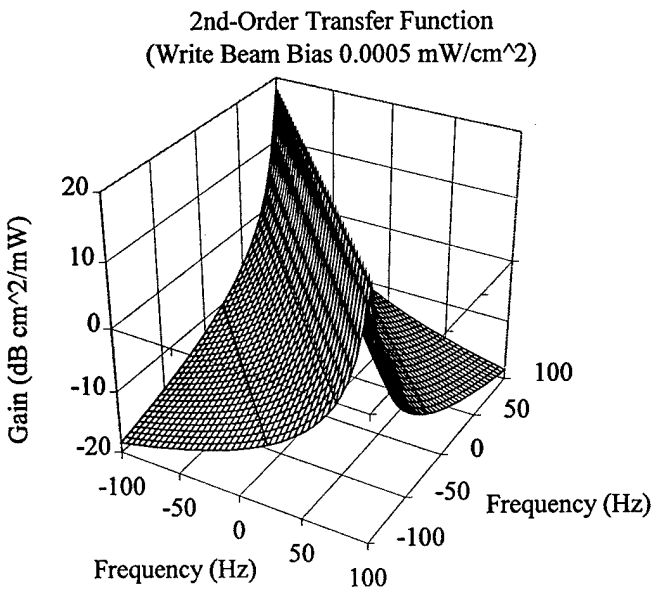

Figure 17: Estimated LCLV complete Write Beam 2nd Order Transfer Function ($\boldsymbol{H}_{11}$).

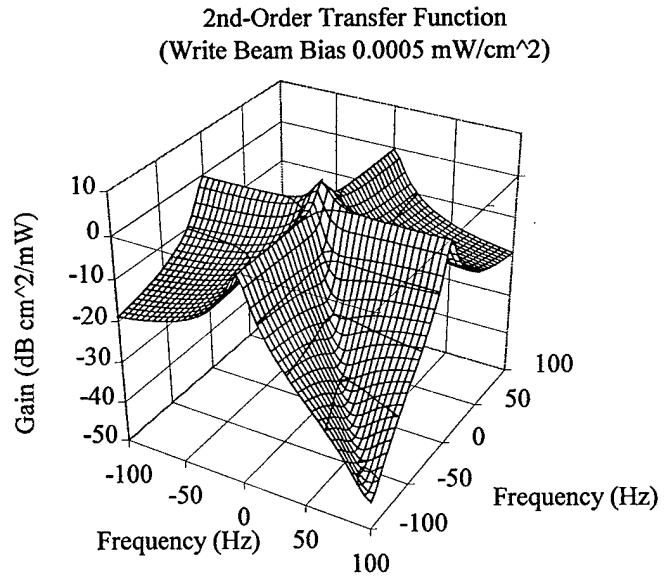

Figure 18: Estimated LCLV Write Beam - Read Beam 2nd

Order Transfer Function ($\boldsymbol{H}_{12}$).

Noise characterization of a liquid crystal light valve using a multiple-port Volterra series model

Mark Storrs, David J. Mehrl, John F. Walkup, Thomas F. Krile

Texas Tech University
Department of Electrical Engineering
Optical Systems Laboratory
Lubbock, TX 79409-3102

ABSTRACT

We present a multiple-input, single-output, weakly nonlinear model of a liquid crystal light valve using a second-order Volterra series and describe an experimental method to measure the nonlinear transfer functions using sinusoidal perturbation and synchronous detection with a lock-in amplifier. Experimentally measured and estimated nonlinear transfer functions are presented. We next discuss the response of the liquid crystal light valve to random inputs and present experimental noise measurements.

Keywords: Spatial Light Modulator, Liquid Crystal Light Valve, Volterra Series, Nonlinear Models.

1. INTRODUCTION

Optical information processing and optical computing systems, while benefiting from high computational speed and a high degree of parallelism, have often suffered from a lack of accuracy. In some applications a lack of accuracy may be tolerated, however progress in optical computing requires an improvement in accuracy[1]. Accuracy may be improved by developing better models of optical devices, then using these models to optimize system design. Developing accurate models of optical devices is complicated by the multiple-port nature of these devices and the nonlinear characteristics they exhibit. We approach this need for improved device models by developing a multiple-port Volterra series model of optical devices. This paper presents an explicit mathematical model of a liquid crystal light valve (LCLV) that views the LCLV as a "black box" that may be adequately described by a mathematical transformation that relates the inputs to the outputs. In applying this approach we recognize that the LCLV is a multiple-input, single-output nonlinear device. We measure the parameters of this model by sinusoidal perturbation with synchronous detection techniques. Optical information processing has suffered from inadequate noise models of the components that comprise optical information processing systems. We next consider the LCLV with random inputs and present the relationship between input and output power spectral density.

2. VOLTERRA SERIES MODEL

In the model we posit for the liquid crystal light valve, the inputs and the output are related by a nonlinear transformation. It is unlikely that this transformation may be expressed exactly in a closed form. Because of this we seek a series approximation of the nonlinear transformation. For static devices a Taylor series expansion about an operating point may be sufficient. This in effect models the device as a memoryless nonlinear system where the output is dependent only on the value of the inputs at each instant. This is too restrictive and certainly will not lead to an accurate model of the LCLV. Consequently we must consider models that incorporate memory. To incorporate memory into the model, we consider the nonlinear transfer function (Volterra Series).

Nonlinear systems with memory may be formulated in a manner that is analogous to that of linear time invariant systems. In fact linear systems are a special case of a class of problems that may be described as "generalized Fock spaces"[2]. These are Hilbert Spaces with "problem-dependent" weighted inner products and include the Volterra series. In this framework, linear and nonlinear theory can be unified. This formulation, using the Volterra series, allows one to determine the output of a nonlinear system given arbitrary inputs using convolution techniques[3] and Laplace transform techniques[4]. The Volterra Series is a generalization of the Taylor series,[5,6] and has been called a "Taylor series with memory"[7]. A Volterra series expansion can be shown to exist for a large class of time invariant[8] nonlinear systems.

The three-input, single-output, second-order Volterra description of a LCLV is depicted as a block diagram in Figure 1. The inputs are identified $x_1(t)$, $x_2(t)$ and $x_3(t)$. Each of the blocks in the system is defined by a nonlinear impulse response, also known as the Volterra kernel. This model includes a first-order component for each input [$h_1(\tau)$, $h_2(\tau)$, $h_3(\tau)$], a second-order component of each input [$h_{11}(\tau_1,\tau_2)$, $h_{22}(\tau_1,\tau_2)$, $h_{33}(\tau_1,\tau_2)$] and a second-order cross-term for each pair of inputs [$h_{12}(\tau_1,\tau_2)$, $h_{23}(\tau_1,\tau_2)$, $h_{31}(\tau_1,\tau_2)$]. The output of each of these components is denoted $y_{mn}(t)$. The system output, $y(t)$ is the summation of these components.

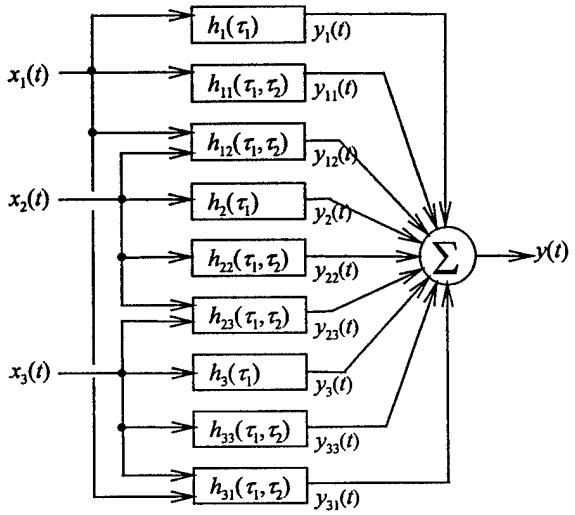

Figure 1: Block diagram of a Volterra series model of a spatial light modulator.

The output of each of the components in the system is defined by convolution integrals. The output of the first order component is given by

$$y_1(t) = \int_{-\infty}^{\infty} h_1(\tau_1)\, x_1(t-\tau_1)\, d\tau_1 \,. \tag{1}$$

We recognize this as the conventional convolution integral describing the output of a linear, time-invariant system. As with linear systems, the nonlinear impulse response for causal system must be zero for any arguments less than zero. The output of the second-order order component is given by the two-dimensional convolution integral

$$y_{11}(t) = \iint_{-\infty}^{\infty} h_{11}(\tau_1,\tau_2)\, x_1(t-\tau_1)\, x_1(t-\tau_2)\, d\tau_1\, d\tau_2 \,. \tag{2}$$

The second-order Volterra kernel is symmetric with respect to τ_1 and τ_2 such that $h_{11}(\tau_1,\tau_2) = h_{11}(\tau_2,\tau_1)$. If an unsymmetrical kernel is derived for a system, there is a process to determine the equivalent symmetrical kernel. In addition the bounded input stability of Volterra kernels is assured if the kernels are absolutely integrable. The output of the second-order cross terms is given by

$$y_{12}(t) = \iint_{-\infty}^{\infty} h_{12}(\tau_1,\tau_2)\, x_1(t-\tau_1)\, x_2(t-\tau_2)\, d\tau_1\, d\tau_2 \,, \tag{3}$$

which shares the symmetry properties of the second-order, single-input kernel. Just as in linear time invariant systems, these nonlinear impulse response functions can be Fourier transformed into multidimensional transfer functions[5,9]: The existence of these transforms is assured for stable Volterra kernels. The first-order, transfer function is given by the conventional Fourier transform of the first-order Volterra kernel as follows:

$$H_1(f_1) = \int_{-\infty}^{\infty} h_1(\tau_1) \exp[-j2\pi f_1 \tau_1]\, d\tau_1 . \tag{4}$$

The second-order, nonlinear transfer function is given by the two-dimensional Fourier transform

$$H_{11}(f_1, f_2) = \int_{-\infty}^{\infty}\int h_{11}(\tau_1, \tau_2) \exp[-j2\pi (f_1\tau_1 + f_2\tau_2)]\, d\tau_1\, d\tau_2 . \tag{5}$$

Because the second-order Volterra kernel $h_{11}(\tau_1, \tau_2)$ is symmetric with respect to τ_1 and τ_2, the transfer function is symmetric with respect to f_1 and f_2, such that $H_{11}(f_1, f_2) = H_{11}(f_2, f_1)$. Since the Volterra kernel $h_n(\tau_1, \tau_2)$ is real, the complex conjugate of the second-order transfer function is $H_{11}^*(f_1, f_2) = H_{11}(-f_1, -f_2)$. Combining the symmetry and complex conjugate properties of the second-order transfer function reveals[10] $H_{11}^*(f, -f) = H_{11}(-f, f) = H_{11}(f, -f)$. This demonstrates that $H_{11}(-f, f)$ is a real valued even function with a phase of zero for all f. The second-order, cross-term transfer function is given by

$$H_{12}(f_1, f_2) = \int_{-\infty}^{\infty}\int h_{12}(\tau_1, \tau_2) \exp[-j2\pi (f_1\tau_1 + f_2\tau_2)]\, d\tau_1\, d\tau_2 . \tag{6}$$

This transfer function shares the symmetry and conjugate properties of the single-input second-order transfer function.

This model may be applied to a LCLV by first identifying the input and output ports. A functional diagram of a Hughes 4050 LCLV is shown in Figure 2. The device has three inputs; the write light (x_1), the read light (x_2) and a 5 kHz AC drive signal (x_3). The LCLV is an optically addressed spatial light modulator that operates by spatially modulating the polarization state of the read light. Amplitude modulation is achieved by using a polarization analyzer[11]. This provides a single output (y). When the write side of the device is illuminated (with coherent or incoherent light) the photosensor becomes conductive with a spatial pattern dependent upon the spatial intensity distribution of the write light. Where the photosensor is conductive, a voltage is impressed across the liquid crystal layer. This voltage causes the liquid crystal molecules to tilt in the direction of the electrodes. The degree of tilt is dependent on the voltage across the liquid crystal, which in turn is dependent upon the intensity of the write light. Linearly polarized incident light on the read side of the device will be transformed into elliptically polarized light with the degree of ellipticity dependent upon the tilt of the liquid crystal molecule. The reflected light now has a polarization component parallel to the orientation of the polarization analyzer that will be passed. The intensity of the light passed by the polarization analyzer is thus dependent on the intensity of the write light.

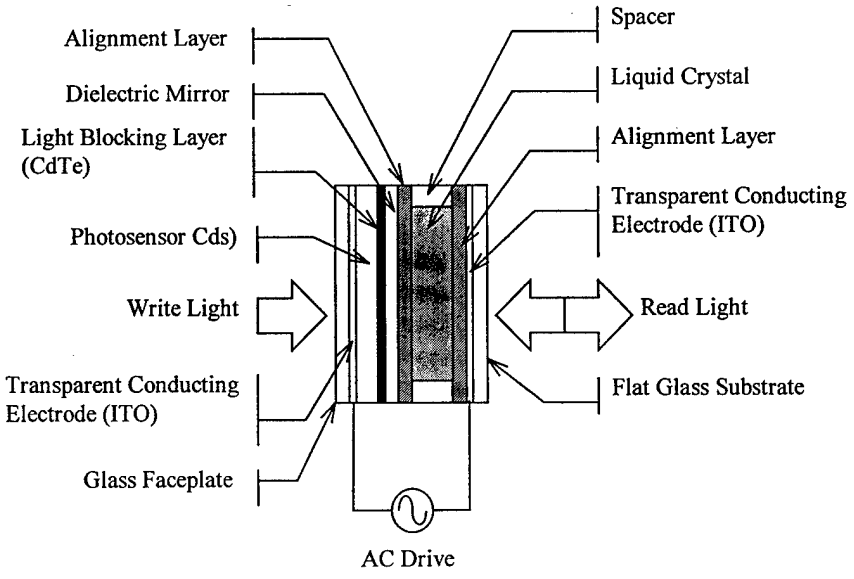

Figure 2: Liquid Crystal Light Valve (LCLV).

3. MEASUREMENT OF NONLINEAR TRANSFER FUNCTIONS

We use a frequency domain measurement method using sinusoidal inputs to directly measure the nonlinear transfer functions using synchronous detection with a lock-in amplifier. When an input to the system is sinusoidally modulated at frequency f, the output of the system will contain components at frequency f and harmonics of f. Provided the system is weakly nonlinear, the higher harmonics do not contribute greatly to the output signal. Each of the frequency components will be proportional to the various nonlinear transfer functions in the Volterra series[12]. The first-order transfer functions will reside at the fundamental frequency. The second-order transfer functions will reside at twice the fundamental frequency. Measuring the second-order cross-term transfer functions requires that two inputs be modulated at differing frequencies. The transfer function will reside at the sum (or difference) of the two input frequencies. These frequency components may be measured with a dual-phase lock-in amplifier by simply referencing the lock-in amplifier to the desired frequency. The phase angle as well as the magnitude of the nonlinear transfer function may be measured using this process. The nonlinear transfer functions that may be measured by this method are summarized in Table 1.

Table 1: Measurement of Nonlinear Transfer Functions.

	1st-Order		2nd-Order		2nd-Order Cross-Term	
	NTF	Frequency	NTF	Frequency	NTF	Frequency
Write Beam Frequency: f_W	$H_1(f)$	f_W	$H_{11}(f_1,f_2)$	$2f_W$	$H_{12}(f_1,f_2)$	f_W+f_R
Read Beam Frequency: f_R	$H_2(f)$	f_R	$H_{22}(f_1,f_2)$	$2f_R$	$H_{23}(f_1,f_2)$	f_R+f_{AC}
AC Drive Frequency: f_{AC}	$H_3(f)$	f_{AC}	$H_{33}(f_1,f_2)$	$2f_{AC}$	$H_{31}(f_1,f_2)$	$f_{AC}+f_W$

With a single sinusoid we can measure the second-order Volterra transfer function only along the line $f_1 = f_2$. To measure the transfer function across the entire frequency plane we must apply a sum of two sinusoids at differing frequencies. The complete second-order Volterra transfer function may be measured by perturbing an input with a sum of two sinusoids and referencing the lock-in amplifier to the sum (or difference) of those frequencies. By judicious selection of the frequencies f_W, f_R and f_{AC} each of the signal components will exist at distinct frequencies Ideally, the frequencies should be incomensurate, however in practice it is sufficient that they be judiciously chosen so as to assure reasonable mutual separation of all frequency terms. In addition, because of the symmetry relationships, it is only necessary to measure data points in only one-fourth of the frequency plane.

An experimental setup to perform the lock-in amplifier measurement is shown in Figure 3. An argon ion laser beam is first conditioned by a laser intensity stabilizer then enters the experimental setup at the upper left corner. A beam splitter is positioned to divide the beam into a write beam and a read beam. An acousto-optic (AO) cell is positioned in each of the beams to provide intensity modulation of the beams. The write and read beams are expanded and passed through a 3mm iris to achieve a beam cross section of relatively constant intensity. A pair of polarizers is positioned in both the write and read beams to provide control over the intensity of the beams and to ensure linear polarization of the read beam. A beamspliter is positioned in both the write and read beams to allow measurement of the inputs to the LCLV with photodiodes. Lenses are positioned to image the iris aperture onto the LCLV write and read surfaces. A crossed polarizer is positioned to provide intensity modulation of the read beam, which is then trained onto a photodiode.

Preliminary measurements were made with unmodulated write and read beam. The static gain of the LCLV is shown in Figure 4. The device shows a monotonically increasing range of operation at low write beam intensity and saturation effects at higher write beam intensity. We note that near the midpoint of the monotonically increasing range it is quite reasonable to posit that the operation of the LCLV may be approximated by a second-order system. The output beam intensity is modulated by the 5 kHz AC drive signal. The first-order modulation is shown in Figure 5 and the second-order modulation is shown in Figure 6. These curves represent the output power residing at the AC drive frequency (and second harmonic) as a fraction of the read beam intensity. The light modulation mechanism producing these effects is the "wobble" of the liquid crystal molecules in response to the AC drive signal. This "wobble" produces a temporal modulation of the polarization state of the reflected light, which is seen in a temporal modulation of the intensity of the light passed by the polarization analyzer. Since the liquid crystal is an induced dipole, the molecules tilt with both halves of the AC cycle, producing a modulation of the read light at twice the AC drive signal frequency. We note that at some levels of write beam intensity the second-order effects are more significant than the first-order effects.

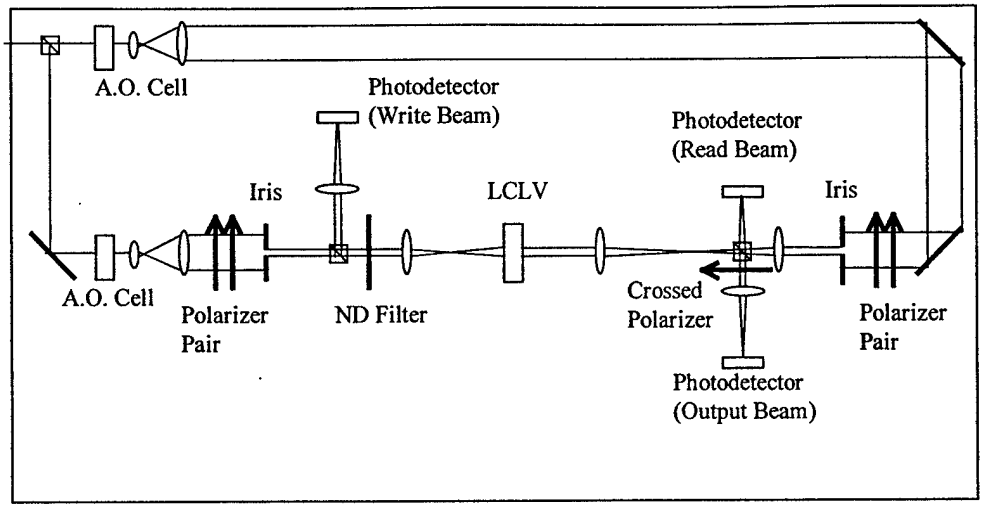

Figure 3: Experimental setup to measure LCLV model parameters.

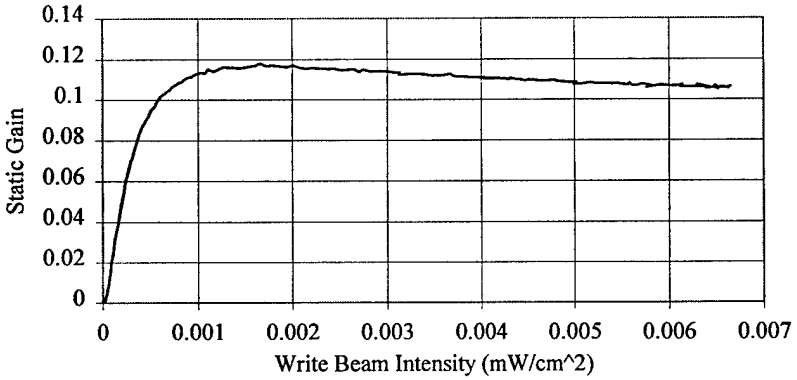

Figure 4: LCLV Static Gain.

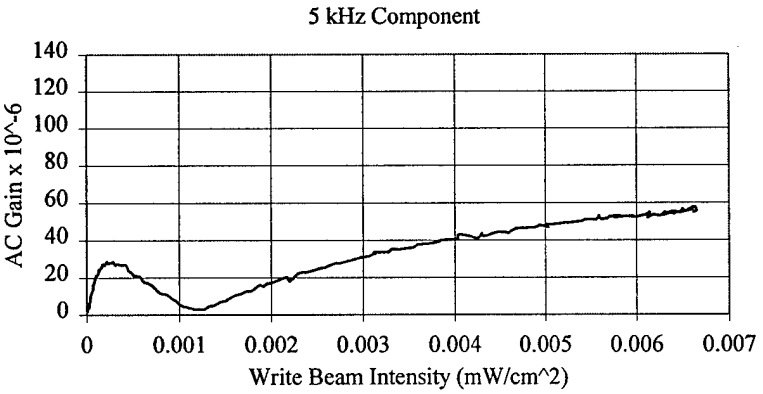

Figure 5: LCLV AC Drive 1st Order Transfer Function (H_3).

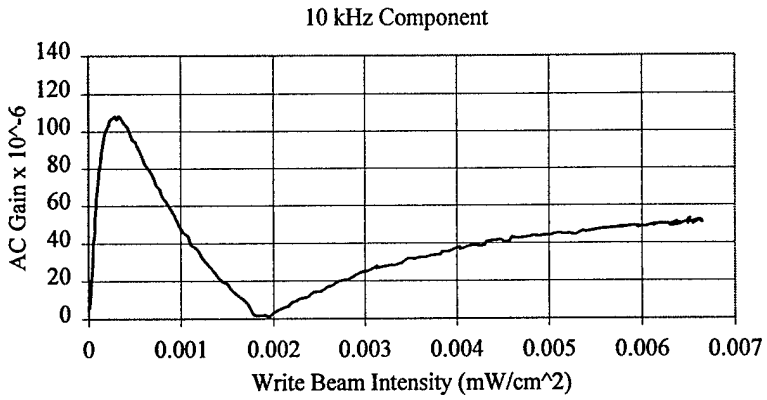

Figure 6: LCLV AC Drive 2nd Order Transfer Function (H_{33}).

To measure the remaining transfer functions, we set the write beam intensity at about the midpoint of the monotonically increasing range, approximately 0.005 mW/cm^2. Modulation of the read beam showed a flat wideband first-order response shown in Figure 7. The LCLV shows a negligible second-order response to read beam modulation. These results indicate a negligible interaction between the read beam and liquid crystal molecules. The response to write beam modulation is very different. The first-order write beam response is shown in Figure 8 and the second-order response is shown in Figure 9. Measured data is shown in the dark line superimposed upon an estimated transfer function. The first-order curve is approximately that of a single pole lowpass filter with a cutoff frequency of about 6 Hz. The second-order curve is approximately that of a second-order single pole lowpass filter with a cutoff frequency of 3 Hz. We note that the second-order transfer function is two-dimensional and this measurement only detects data points along the line $f_1 = f_2$. Since the response curve drops at 20 dB per decade (as opposed to 40 dB per decade), the second-term may be modeled as a squaring operation followed by a low-pass filter. The complete second-order transfer function can be shown to take the form

$$H_{11}(f_1, f_2) = H(f_1 + f_2), \tag{7}$$

where H(f) represents the low-pass filter transfer function. Using the estimated transfer function curve shown in Figure 9. the estimated complete second-order transfer function is shown in Figure 10. In lieu of direct measurement of the second-order cross-term transfer functions, they may be approximated from our knowledge of the LCLV operation. Since the output beam intensity is directly scaled by the read beam intensity, the modulated output beam intensity is also directly scaled by the read beam intensity. In effect this produces a multiplication operation between the write beam and the read beam. The second-order cross-term transfer function can be shown to take the form

$$H_{12}(f_1, f_2) = H_1(f_1) H_2(f_2). \tag{8}$$

Applying this relationship to the transfer functions shown in Figures 8 and 9, and making the function symmetrical with respect to f_1 and f_2, results in the second-order transfer function shown in Figure 11. The same relationship will hold between the AC drive and the two optical beams. The second order transfer function H_{23} will be the same form as Figure 9, scaled by H_3 (-47 dB in this case) and shifted to a base frequency of 5 kHz. The second order transfer function H_{31} will be the same form as Figure 14, scaled and shifted in a similar manner.

4. NOISE CHARACTERIZATION

Our interests in noise characterization are both the noise transformation characteristics of the LCLV and the noise generation characteristics of the LCLV. The experimental setup show in Figure 3 was used in these measurements. Preliminary noise measurements were made by modulating the write and read beam with a random noise source. The write beam, read beam, AC drive and output beam signals were sampled with an A/D converter at 50000 samples per second and were stored for analysis. Signal-to-noise ratios were calculated for the write beam, read beam and output beam signals. The results of these measurements are shown in Table 2. Four different experiments are reflected in these results, each shows different aspects of the noise characteristics of the LCLV.

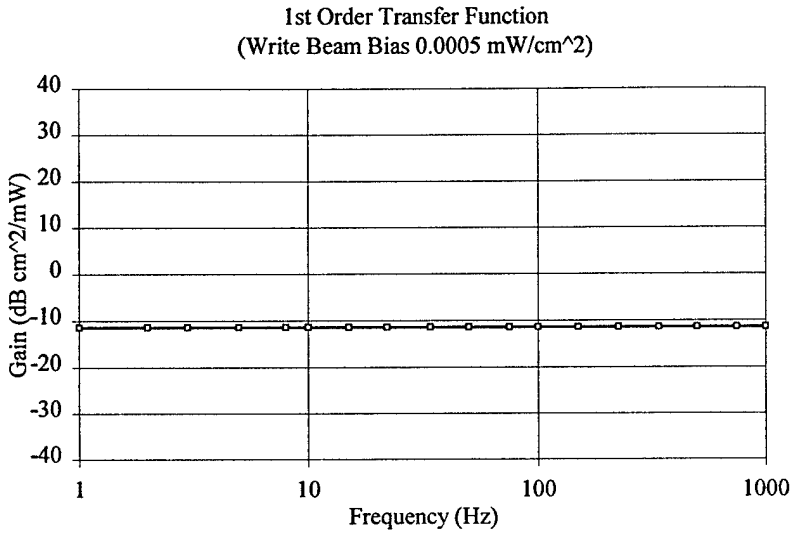

Figure 7: LCLV Read Beam 1st Order Transfer Function (H_2).

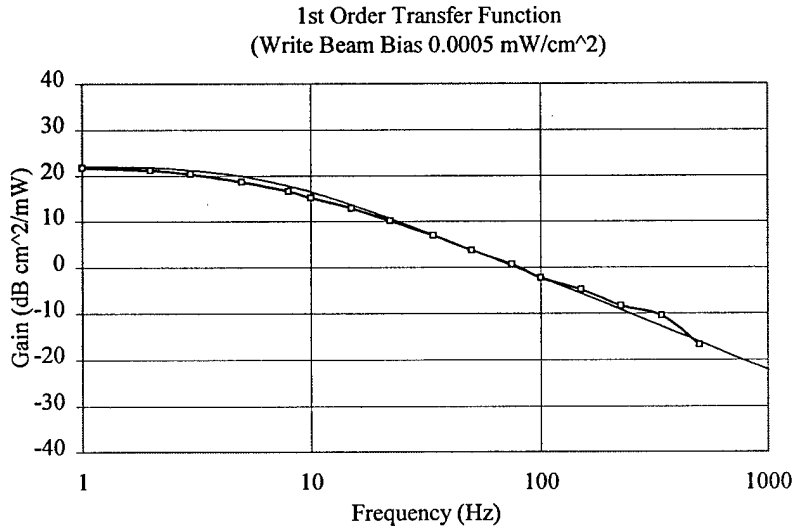

Figure 8: LCLV Write Beam 1st Order Transfer Function (H_1).

In the first experiment we impressed no noise signal upon the write beam or the read beam. The beams did bear laser noise and noise from extraneous sources, such as vibration. The write beam displays a very high signal-to-noise ratio and the read beam a moderately high signal-to-noise ratio. We note that the output beam has a reduced signal-to-noise ratio, indicating noise generation within the LCLV. The source of the noise is the 5 kHz and 10 kHz modulation due to the AC drive signal.

The second experiment was conducted with a random signal source modulating the write beam and the read beam unmodulated. A portion of the write beam time signal and power spectral density is shown in Figure 12. The signal has significant frequency components to 1 kHz. The write beam has a low signal-to-noise ration and the read beams shows a very high signal-to-noise ratio. The output beam shows increased noise levels, but still demonstrates a high signal-to-noise ratio. This is attributed to the lowpass filtering characteristic (see Figure 8) applied to the write beam. A great part of the noise present in the output beam is again attributed to the AC drive.

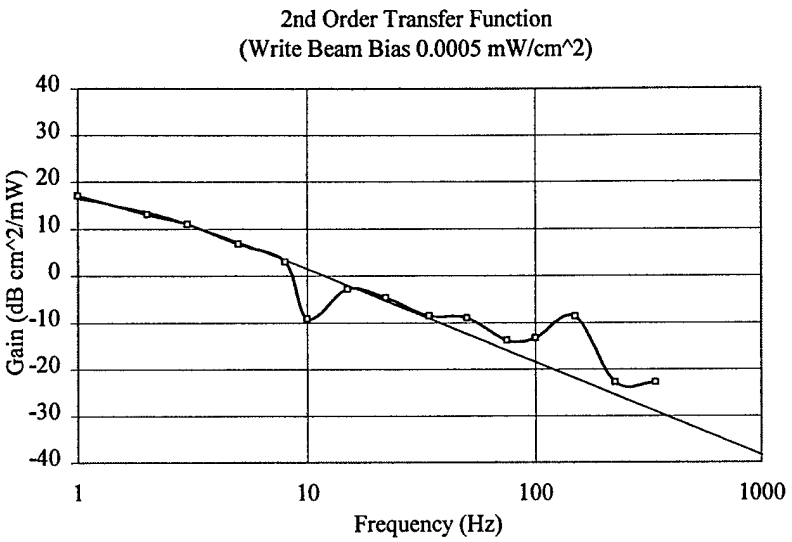

Figure 9: LCLV Write Beam 2nd Order Transfer Function (H_{11}).

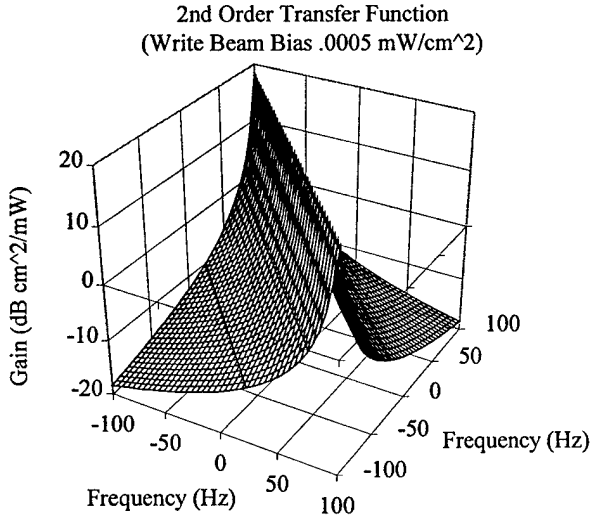

Figure 10: Estimated LCLV Complete Write Beam 2nd Order Transfer Function (H_{11}).

In the third experiment the read beam was modulated with a random noise source and the write beam was unmodulated. A portion of the read beam time signal and power spectral density is shown in Figure 13. The signal has significant frequency components to higher than 3 kHz. The read beam has a low signal-to-noise ratio and the read beam shows a very high signal to noise ratio. Interestingly the output beam shows a small improvement in signal-to-noise ratio. This indicates lowpass filtering of the read beam. Our measurements shown in Figure 6 indicate a flat response from 1 Hz to 1 kHz. Apparently the transfer function attenuates higher frequencies. The improvement in signal-to-noise ratio is attributed to the attenuation of high frequencies. This effect is more significant than the noise generated by the AC drive signal.

The fourth experiment was conducted with both the write beam and the read beam modulated by a random noise source. Both the read and the write beam show a low signal-to-noise ratio. The output beam shows an improved signal-to-noise ratio similar to that shown in the third experiment. Again this demonstrates the lowpass filtering of the write beam and the attenuation of higher frequencies of the read beam.

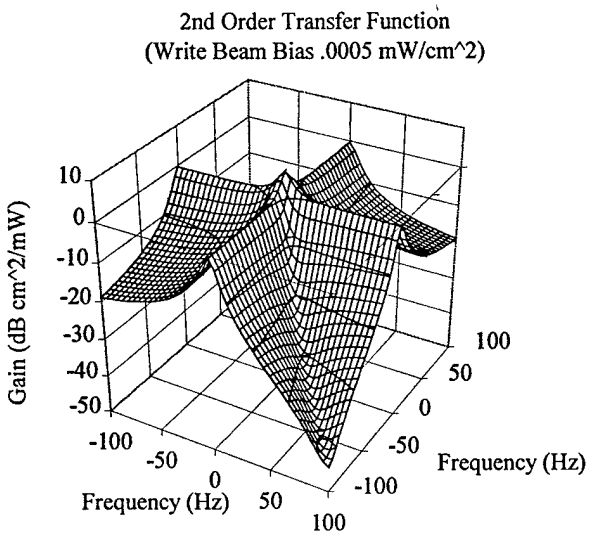

Figure 11: Estimated LCLV Write Beam – Read Beam 2nd Order Transfer Function ($\boldsymbol{H}_{12}$).

Table 2: Preliminary LCLV Noise Measurement.

Experiment Description	Write Beam SNR	Read Beam SNR	Output Beam SNR
1. No Write or Read beam modulation	159	73	60
2. Write beam modulated	20	293	210
3. Read beam modulated	503	16	19
4. Write and Read beam modulated	17	16	19

The Volterra series model may be used to analyze the propagation of noise through the LCLV. By the nature of optical devices, we must consider random inputs about a dc value. In the following discussion the dc component has been subtracted from the inputs x_1 and x_2, and also from the output y. We recall the Volterra series model is the sum of the various Volterra kernels as shown in Figure 1. The power spectral density of the first-order kernels is well know and is given by

$$\boldsymbol{S}_{y_1 y_1}(f) = |\boldsymbol{H}_1(f)|^2 \boldsymbol{S}_{x_1 x_1}(f) . \tag{9}$$

For a zero-mean input the output of the first order kernels is also zero-mean. This is not true of the second-order kernels. The zero-mean power spectral density may be defined by subtracting the non-zero response to a zero-mean random input.[10] The power spectral density of the second-order kernel then takes the form

$$\boldsymbol{S}_{y_{11} y_{11}}(f) = 2\int_{-\infty}^{\infty} |\boldsymbol{H}_{11}(f_1, f-f_1)|^2 \boldsymbol{S}_{x_1 x_1}(f_1)\boldsymbol{S}_{x_1 x_1}(f-f_1)\, df_1 . \tag{10}$$

The second-order cross-term kernels can be shown to have a similar zero-mean power spectral density that incorporates two inputs as follows:

$$\boldsymbol{S}_{y_{12} y_{12}}(f) = \int_{-\infty}^{\infty} |\boldsymbol{H}_{12}(f_1, f-f_1)|^2 \boldsymbol{S}_{x_1 x_1}(f_1)\boldsymbol{S}_{x_2 x_2}(f-f_1)\, df_1 . \tag{11}$$

From these results, the power spectral density of each of the Volterra kernels may be determined provided we know the power spectral density of each of the inputs (either random or sinusoidal) and the magnitude squared of each of the nonlinear transfer functions. To determine the power spectral density of the total Volterra system we first determine the autocorrelation of the system output. This is given by

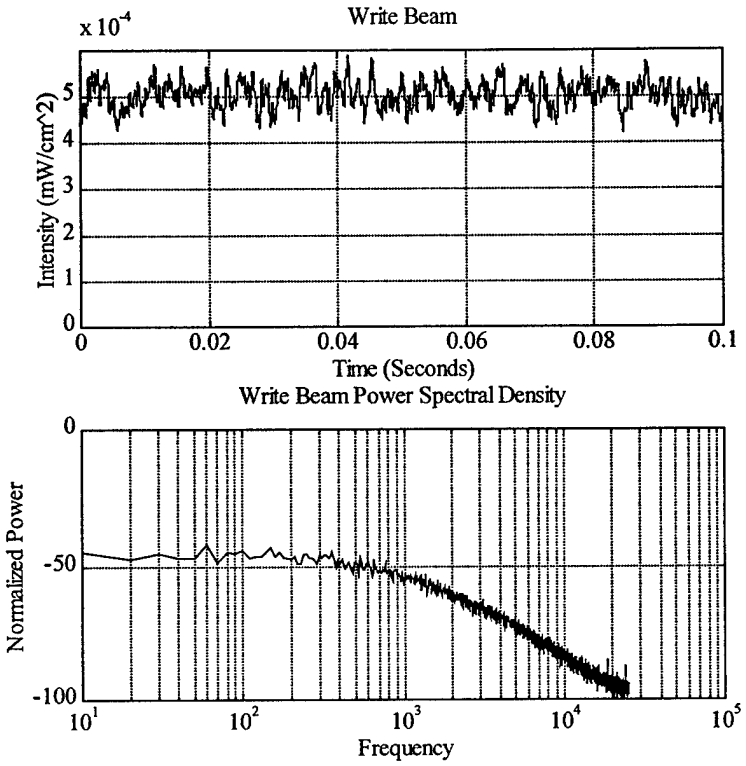

Figure 12: Write Beam Time Signal and Power Spectral Density.

$$R_{yy}(\tau) = \mathrm{E}[y(t)y(t+\tau)]\,, \tag{12}$$

where $y(t)$ is the sum of the linear, second-order and second-order cross terms $\mathrm{E}[\cdot]$ is the expectation operator. Explicitly showing these sums reveals

$$R_{yy}(\tau) = \mathrm{E}\left\{[y_1(t) + y_{11}(t) + \cdots + y_{31}(t)] \times [\,y_1(t+\tau) + y_{11}(t+\tau) + \cdots + y_{31}(t+\tau)]\right\} \tag{13}$$

Carrying out the multiplication results in eighty-one terms, most of which result in zero contribution. In determining this we assume that the inputs statistically independent, zero-mean, wide sense stationary and ergotic. Those that remain and contribute to the autocorrelation are included in

$$R_{yy}(\tau) = R_{y_1y_1}(\tau) + R_{y_{11}y_{11}}(\tau) + R_{y_{12}y_{12}}(\tau) + R_{y_2y_2}(\tau) + R_{y_{22}y_{22}}(\tau) + R_{y_{23}y_{23}}(\tau) + R_{y_3y_3}(\tau) + R_{y_{33}y_{33}}(\tau) + R_{y_{31}y_{31}}(\tau)\,. \tag{14}$$

The spectral power density of the output is simply the Fourier transform of the autocorrelation and is given by

$$\boldsymbol{S}_{yy}(\tau) = \boldsymbol{S}_{y_1y_1}(\tau) + \boldsymbol{S}_{y_{11}y_{11}}(\tau) + \boldsymbol{S}_{y_{12}y_{12}}(\tau) + \boldsymbol{S}_{y_2y_2}(\tau) + \boldsymbol{S}_{y_{22}y_{22}}(\tau) + \boldsymbol{S}_{y_{23}y_{23}}(\tau) + \boldsymbol{S}_{y_3y_3}(\tau) + \boldsymbol{S}_{y_{33}y_{33}}(\tau) + \boldsymbol{S}_{y_{31}y_{31}}(\tau)\,. \tag{15}$$

Each of these terms is defined in Eq. 9, 10 or 11.

The power spectral density of a LCLV excited by random inputs in the write and read beams is shown in Figure 14. The inputs are shown in Figures 12 and 13. Qualitatively , the output appears to have similar time and spectral properties as the read beam. This indicates that the dominant term in the Volterra series is the first-order read beam term [$\boldsymbol{H}_2(f)$]. Since the read beam contained frequencies up to 3 kHz and above, the contribution of the AC drive signal, detected at 5 kHz and 10 kHz is minimal.

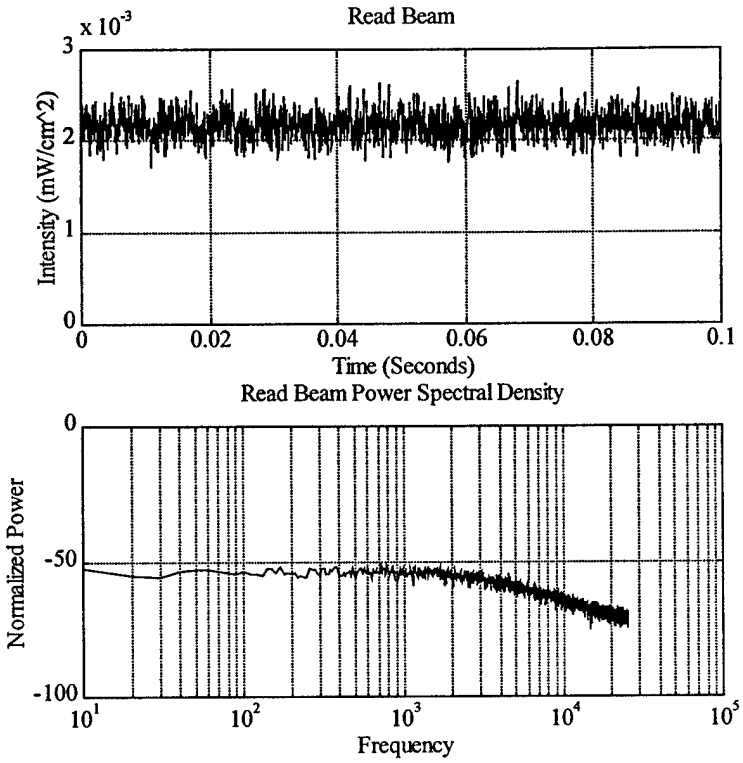

Figure 13: Write Beam Time Signal and Power Spectral Density.

5. CONCLUSIONS

The Volterra series is capable of representing weakly nonlinear, multiple-input, single-output systems. The Volterra kernels may be measured through straightforward techniques. The measured quantities are directly applicable to the spectral analysis and noise characterization of the nonlinear device. The Volterra series is a reasonable model for the LCLV and provides a tool to analyze the noise properties of the device.

6. ACKNOWLEDGEMENTS

This research was funded by the Air Force Office of Scientific Research under the Augmentation Awards for Science and Engineering Research Training (AASERT) Grant F49620-95-1-0402.

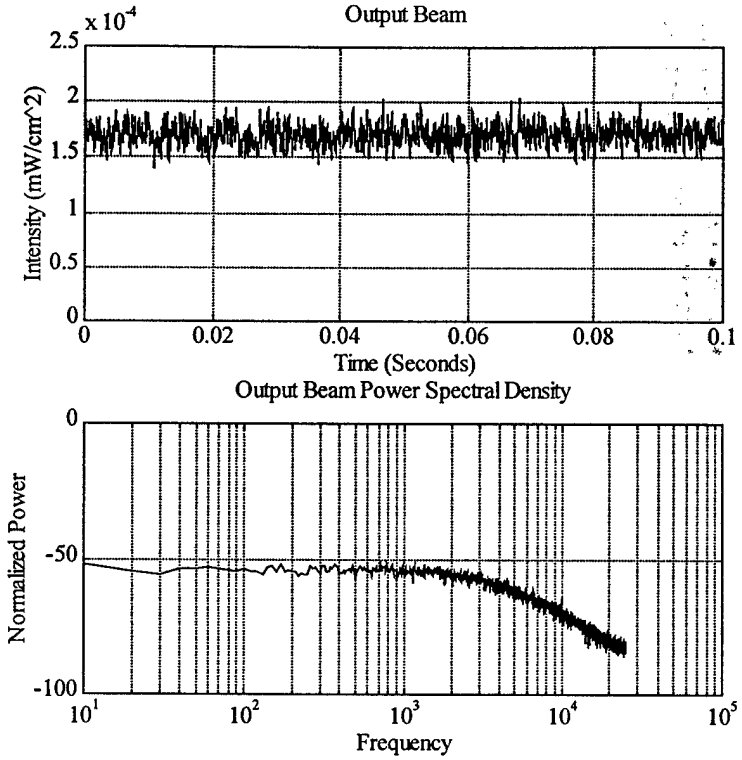

Figure 14: Output Beam Time Signal and Power Spectral Density.

7. REFERENCES

1. S. G. Batsell, T. L. Jong, J. F. Walkup and T. F. Krile, "Noise limitations in optical linear algebra processors," *Applied Optics*, **29**, 2084-2090 (1990).
2. R. J. P. De Figueiredo, "A Generalized Fock Space Framework for Nonlinear System and Signal Analysis," *IEEE Transactions on Circuits and Systems*, **30**, 637-647 (1983).
3. I. W. Sandburg, "A Perspective on System Theory," *IEEE Transactions on Circuits and Systems*, **31**, 88-103 (1984).
4. W. J. Rugh, *Nonlinear System Theory: The Volterra/Wiener Approach*, Johns Hopkins University Press, Baltimore, Maryland (1981).
5. M. Schetzen, *The Volterra and Wiener Theories of Nonlinear Systems*, John Wiley and Sons, Inc., New York (1980).
6. M. Schetzen, "Nonlinear System Modeling Based on the Wiener Theory," *Proceedings of the IEEE*, **69**, 1557-1573 (1981).
7. E. Bedrosian and S. O. Rice, "The Output Properties of Volterra Systems (Nonlinear Systems with Memory) Driven by Harmonic and Gaussian Inputs," *Proceedings of the IEEE*, **59**, 1688-1707 (1971).
8. I. W. Sandburg, "Expansions for Nonlinear Systems," *The Bell System Technical Journal*, **61**, 159-199 (1982).
9. J. C. Peyton Jones and S. A. Billings, "Interpretation of non-linear frequency response functions," *International Journal of Control*, **52**, 319-346 (1990).
10. J. S. Bendat, *Nonlinear System Analysis and Identification from Random Data*, John Wiley and Sons, Inc., New York (1990).
11. W. P. Bleha, L. T. Lipton, E. Wiener-Avnear, J. Grinberg, P. G. Reif, D. Casasent, H. B. Brown and B.V. Markevitch, "Application of the Liquid Crystal Light Valve to Real-Time Optical Data Processing," *Optical Engineering*, **17**, 371-384 (1978).
12. M. Storrs, D. J. Mehrl, J. F. Walkup and T. F. Krile, "Volterra series modeling of spatial light modulators," submitted for publication in *Applied Optics*.